

Controlling the Biological Fate of Micellar Nanoparticles: Balancing Stealth and Targeting

Journal:	<i>ACS Nano</i>
Manuscript ID	nn-2020-06033s.R3
Manuscript Type:	Article
Date Submitted by the Author:	09-Sep-2020
Complete List of Authors:	<p>Sivaram, Amal; University of Queensland Australian Institute for Bioengineering and Nanotechnology; The Centre for Advanced Imaging; The University of Queensland</p> <p>Wardiana, Andri; University of Queensland Australian Institute for Bioengineering and Nanotechnology</p> <p>Alcantara, Sheilajen ; University of Melbourne, Microbiology and Immunology; University of Melbourne, Microbiology and Immunology</p> <p>Sonderegger, Stefan; University of Queensland Australian Institute for Bioengineering and Nanotechnology</p> <p>Fletcher, Nicholas; University of Queensland, Centre for Advanced Imaging; The Centre for Advanced Imaging; The University of Queensland</p> <p>Houston, Zachary; University of Queensland Australian Institute for Bioengineering and Nanotechnology; The Centre for Advanced Imaging; The University of Queensland</p> <p>Howard, Christopher; University of Queensland Australian Institute for Bioengineering and Nanotechnology; The University of Queensland</p> <p>Mahler, Stephen; University of Queensland, Australian Institute of Bioengineering & Nanotechnology; The University of Queensland</p> <p>Alexander, Cameron; University of Nottingham, School of Pharmacy</p> <p>Kent, Stephen; University of Melbourne; University of Melbourne, Microbiology and Immunology</p> <p>Bell, Craig; University of Queensland, Australian Institute for Bioengineering and Nanotechnology; The Centre for Advanced Imaging; The University of Queensland</p> <p>Thurecht, Kristofer; The University of Queensland, Australian Institute for Bioengineering and Nanotechnology; The University of Queensland, Centre for Advanced Imaging; The University of Queensland; The University of Queensland</p>

Controlling the Biological Fate of Micellar Nanoparticles: Balancing Stealth and Targeting

Amal J. Sivaram^{1,2,3}, Andri Wardiana¹, Sheilajen Alcantara⁵, Stefan E. Sonderegger¹, Nicholas L. Fletcher^{1,2,3}, Zachary H. Houston^{1,2,3}, Christopher B. Howard^{1,6}, Stephen M. Mahler^{1,6}, Cameron Alexander⁴, Stephen J. Kent⁵, Craig A. Bell^{1,2,3}, Kristofer J. Thurecht^{1,2,3}*

¹Australian Institute for Bioengineering and Nanotechnology, The University of Queensland, St Lucia, QLD 4072, Australia

²Centre for Advanced Imaging, The University of Queensland, St Lucia, QLD 4072, Australia

³ARC Centre of Excellence in Convergent Bio-Nano Science and Technology, and ARC Training Centre for Innovation in Biomedical Imaging Technology, The University of Queensland, St Lucia, QLD 4072, Australia

⁴School of Pharmacy, The University of Nottingham, Nottingham NG7 2RD, United Kingdom

⁵ARC Centre of Excellence in Convergent Bio-Nano Science and Technology, and the Department of Microbiology and Immunology, The University of Melbourne, at the Peter Doherty Institute for Infection and Immunity, Parkville, Victoria 3010, Australia

⁶ARC Training Centre for Biopharmaceutical Innovation, The University of Queensland, St Lucia, QLD 4072, Australia

*Corresponding author, E-mail: k.thurecht@uq.edu.au (Kristofer J. Thurecht)

ABSTRACT

Integrating nanomaterials with biological entities has led to the development of diagnostic tools and biotechnology-derived therapeutic products. However, to optimise the design of these hybrid bionanomaterials, it is essential to understand how controlling the biological interactions will influence desired outcomes. Ultimately, this knowledge will allow more rapid translation from the bench to the clinic. In this paper, we developed a micellar system that was assembled using modular antibody-polymer amphiphilic materials. The amphiphilic nature was established using either polyethylene glycol (PEG) or a single-chain variable fragment (scFv) from an antibody as the hydrophile, and a thermoresponsive polymer (poly(oligoethylene glycol) methyl ether methacrylate) as the hydrophobe. By varying the ratios of these components, a series of nanoparticles with different antibody content was self-assembled, where the surface presentation of targeting ligand was carefully controlled. *In vitro* and *in vivo* analysis of these systems identified a mismatch between the optimal targeting ligand density to achieve maximum cell association *in vitro* compared to tumour accumulation *in vivo*. For this system, we determined an optimum antibody density for both longer circulation and enhanced targeting to tumours that balanced stealthiness of the particle (to evade immune recognition as determined in both mouse models and in whole human blood) with enhanced accumulation achieved through receptor binding on tumour cells in solid tumours. This approach provides fundamental insights into how different antibody densities affect the interaction of designed nanoparticles with both target cells and immune cells, thereby offering a method to probe the intricate interplay between increased targeting efficiency *versus* the subsequent immune response to nanoparticles.

1
2
3 **KEYWORDS:** single-chain variable fragment, polyethylene glycol, antibody density, micellar
4 nanoparticles, tumour targeting,
5
6
7
8
9

10 Nanomedicines are now evolving as precisely engineered nanomaterials that offer significant
11 potential to overcome many limitations of conventional anti-cancer drugs.¹ The therapeutic
12 efficacies of current drugs are limited due to unfavourable physicochemical properties such as
13 low solubility, instability, toxicity issues due to lack of selectivity, and poor pharmacokinetics.
14
15 In contrast, the properties of new nanomaterials can be designed to enhance biocompatibility,
16 reduce toxicity, control drug release, and increase circulation time in the body, enabled much
17 improved therapeutic delivery.² Furthermore, nanomaterials offering theranostic features can
18 enable real-time monitoring of site-specific drug delivery to the cancer target.³ Although
19 nanomaterials have been intensively investigated for delivering drugs to the solid tumours,
20 there are studies showing discrepancies with the number of nanoparticles reaching tumour sites
21 *versus* the administered nanoparticle dose. In a meta-analysis of a wide range of nanomedicines
22 administered to mice, it was suggested that on average only 0.7% of the injected dose is retained
23 in the solid tumours, indicating the exceptional challenge for translation of nanomedicines.⁴
24
25 In order to enhance delivery efficiency, it is vital to understand the factors that influence the
26 pharmacokinetic profile and behaviour of nanomaterials. Upon intravenous administration,
27 nanoparticles initially interact with blood components before distributing throughout the
28 various tissues, including the target tumour site. Longer blood circulation times are a critical
29 factor in achieving successful tumour accumulation, which ultimately depends on how well
30 nanoparticles overcome the biological barriers and clearance systems designed to exclude and
31 remove exogenous materials. For nanomaterials, a major problem is rapid coating by opsonin
32 proteins and subsequent clearance by the mononuclear phagocytic system (MPS).^{5,6} The blood
33
34
35
36
37
38
39
40
41
42
43
44
45
46
47
48
49
50
51
52
53
54
55
56
57
58
59
60

1
2
3 residence times of nanoparticles can be influenced by their physicochemical properties such as
4 shape, surface charge, size, and ligand densities.⁷ Nonetheless, an in-depth analysis of the
5 relationships between physicochemical properties, body clearance and the overall targeting
6 efficacies of nanoparticles has yet to be conducted and correlated fully across a coherent set of
7 particles.
8
9

10
11
12
13
14 Research to date has established some rules for consideration when designing nanomaterials
15 for drug delivery. For example, it is well reported that nanoparticle sizes in the range of 20 –
16 30 nm results in higher receptor-mediated uptake, while nanoparticles in the 20 – 100 nm range
17 can be used for enhanced liver accumulation.⁸ However, there is by no means a consensus in
18 the literature as to what is the most ideal size of particle for optimal therapeutic efficiency and
19 most nanoparticle strategies develop materials that span particle sizes between 20-200 nm. It
20 is also well established (but not precisely quantified) that “targeted” nanomaterials show
21 greater uptake and accumulation in cells, mostly under *in vitro* conditions. Often when these
22 studies are translated to animals, however, incorporating a higher density of targeting protein
23 functionality to enhance recognition at an intended disease site increases immune recognition
24 and expedites clearance of nanomaterials; in some cases, such modulation with targeting
25 ligands can actually decrease the tumour accumulation compared to the untargeted
26 nanomedicine.⁹ Despite the wealth of data on new and sophisticated drug delivery vehicles,
27 there are significant exceptions to these generalised rules, and there is no clear methodology
28 for optimising targeting approaches for these materials.¹⁰ Furthermore, these generalised rules
29 that often are used to design new materials seldom transfer between the bench, the cell in a
30 dish, and the body, leading to a disconnect between materials design and observed properties.⁹
31
32
33 One point of significant interest is the influence of targeting ligand density on nanomaterial
34 interactions with cell surface receptors.¹¹ A few studies have investigated how the number and
35
36
37
38
39
40
41
42
43
44
45
46
47
48
49
50
51
52
53
54
55
56
57
58
59
60

1
2
3 density of ligands influence the internalisation and subsequent cellular processing of
4 bionanomaterials, but there is limited information on how the surface density of ligands affects
5 the physiological behaviour of nanomaterials in circulation, and how this ultimately translates
6 to tumour accumulation.^{12,13} Nonetheless, the limited data available suggests that there is a
7 threshold at which clustering of ligands saturates surface receptors, often leading to modified
8 internalisation pathways and variable efficacy of delivered therapeutics.^{14,15} The challenge is
9 to develop strategies to design next-generation nanomaterials, accounting for the competing
10 requirements of enhanced cellular uptake through higher ligand density, with embedded
11 “stealthiness” to avoid rapid immune recognition and clearance. This epitomises the general
12 observation that what is evidenced *in vitro*, is difficult to transition to *in vivo*, due to the absence
13 of the competing requirement for stealthiness in the majority of *in vitro* assays.

14
15 To date, the majority of studies looking at receptor clustering effects have focused on the effect
16 of small molecule ligands, such as the folate receptor.¹⁶ One reason for this is the intrinsic
17 complexity associated with biomolecule assemblies, complicating the development of well-
18 defined systems where this effect can be monitored universally. This project progresses our
19 understanding of targeting in a complex biological environment, through the development of
20 micellar systems specifically designed to control the targeting ligand density of more
21 biologically relevant protein-based ligands through the self-assembly process. This is achieved
22 using thermoresponsive polymers, which can interact with the proteins in aqueous conditions
23 without denaturing them.

24
25 In this study, we synthesised an amphiphilic antibody-polymer conjugate that was self-
26 assembled to form micelles in which the surface constitutes a defined mixture of stealthy
27 polymers and an antibody fragment (single-chain variable fragment – scFv) that shows high
28 affinity for receptors upregulated on cancer cells. The advantage of this approach is that the
29
30
31
32
33
34
35
36
37
38
39
40
41
42
43
44
45
46
47
48
49
50
51
52
53
54
55
56
57
58
59
60

1
2
3 relatively small size of scFvs avoids steric effects associated with whole monoclonal
4 antibodies, affording greater control over packing density, while the polymeric materials offer
5 well-understood physicochemical tuneability that is required to develop such complex, yet
6 ordered systems. By modulating the incorporation of antibody-polymer hybrid amphiphiles
7 through co-assembly with purely synthetic polymer amphiphiles, the density of antibody
8 fragments on the micelle can be manipulated across a significant range. Hence, the effect of
9 ligand density on how the micelles bind to cell surface receptors and how it dictates the cellular
10 uptake pathways of particular nanomaterials can be investigated. This can then be compared to
11 the ultimate biological fate of the micelles upon injection into tumour-bearing mice, where the
12 nanoparticles are exposed to a greater complement of biological barriers that limit tumour
13 accumulation. This offers a robust approach to develop an in-depth understanding of how these
14 fundamental properties can be utilised to enhance cellular uptake and influence biodistribution.
15 Figure 1 schematically represents the hypothesis of this study, that increased antibody will lead
16 to maximum binding efficiency *in vitro*, but also leads to greater immune recognition that often
17 manifests in reduced tumour accumulation.
18
19
20
21
22
23
24
25
26
27
28
29
30
31
32
33
34
35
36
37
38
39
40
41
42
43
44
45
46
47
48
49
50
51
52
53
54
55
56
57
58
59
60

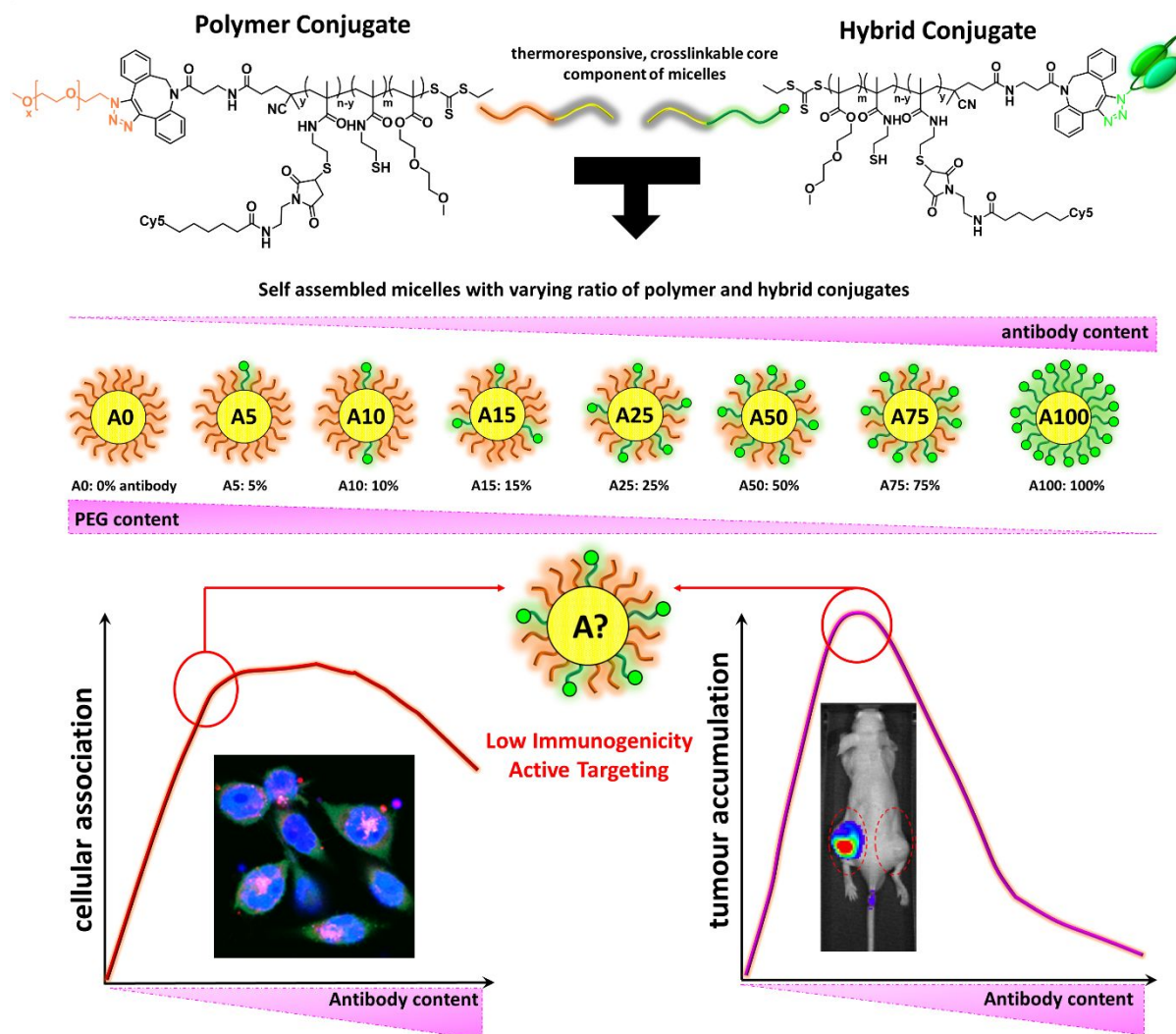


Figure 1. Schematic diagram postulating the influence of ligand density on nanoparticle uptake *in vitro* and *in vivo*. An optimum ratio of antibody to PEG components on micelles may lead to an improvement in the therapeutic efficacy due to enhanced targeting and lower immune response.

RESULTS AND DISCUSSION

We set out to design a nanomaterial system where precise control over the ratio of antibody and PEG components could be achieved, allowing us to synthesise a range of micelles incorporating various antibody densities so we could understand their biological fate. The design elements of this study required a number of important conceptual and materials

1
2
3 advances. First, a synthetic component was required that could be coupled with proteins under
4 aqueous conditions (*i.e.* water-soluble), but which would also act as the hydrophobe for
5 assembly into micelles. It was also necessary to have a mechanism to crosslink the hydrophobic
6 core for enhanced stability of the assemblies. Second, a suitable mechanism for coupling the
7 antibody fragment to the hydrophobe was needed, as well as a defined way of tracking
8 successful incorporation of the different components into the assemblies.
9

10
11 **Thermoresponsive, crosslinkable polymer chain as the hydrophobic component.** A key
12 challenge in the development of amphiphilic polymer-protein conjugates is the stringent
13 reaction conditions required for antibody modifications. For example, such reactions cannot be
14 undertaken in organic solvents (as this leads to loss of tertiary structure); however in water
15 hydrophobic polymers are not soluble, and heterogeneous conjugation is poor yielding and
16 uncontrolled.¹⁷ Thus, we sought to develop a thermoresponsive “hydrophobic” component for
17 the amphiphilic system using di(ethylene glycol) methyl ether methacrylate (DEGMA) and
18 pentafluorophenyl methacrylate (MAPFP) in which coupling to the antibody can be undertaken
19 in water at low temperature, but upon an increase in temperature above the lower critical
20 solution temperature (LCST) the polymer becomes insoluble. To this end, we sought to develop
21 end-functional responsive polymers that also contained a mid-chain reactive group for
22 crosslinking the final micellar assemblies. 4-cyano-4-
23 (ethylsulfanylthiocarbonylsulfanyl)pentanoic acid (CEPA) was employed as the reversible
24 addition-fragmentation chain transfer (RAFT) agent to provide control over the radical
25 copolymerisation of these two monomers as well as impart acid chain-end functionality that
26 could then be modified with a dibenzocyclooctyne (DBCO) amine linker for downstream
27 coupling of the solvent-sensitive antibody fragments through strain promoted alkyne azide
28 cycloaddition (SPAAC).¹⁸ The generalised scheme and selective characterisation of each
29
30
31
32
33
34
35
36
37
38
39
40
41
42
43
44
45
46
47
48
49
50
51
52
53
54
55
56
57
58
59
60

component is presented in Figure 2A. Using CEPA, statistical copolymers of p(DEGMA-*co*-MAPFP) were synthesised with defined molecular weights and dispersities (Table 1). The molecular weights of p(DEGMA-*co*-MAPFP) were calculated using ¹H NMR by integrating the DEGMA side-chain protons at 4.01 – 4.24 ppm (for DEGMA contribution), the p(MAPFP) and p(DEGMA) methyl protons at 0.8 – 1.28 ppm and subtracting the contribution from DEGMA (to calculate the MAPFP contribution), and calibrating to the methylene protons adjacent to the terminal trithiocarbonate (3.22 ppm). ¹H and ¹⁹F NMR spectra of the p(DEGMA-*co*-MAPFP) copolymer can be seen in Figure 2B and 2C, respectively, and SEC results are shown in Table 1.

Table 1. Summary of physicochemical characteristics of the hydrophobic component after each modification.

Si No.	Sample	M_n^a (kDa)	D_M^b	Yield (%)	LCST ^c (°C)
1	p(DEGMA- <i>co</i> -MAPFP)	6.0	1.30	92	10
2	p(DEGMA- <i>co</i> -MACYS)	5.5	1.50	85	16
3	DBCO-p(DEGMA- <i>co</i> -MACYS)	6.5	1.60	82	16

^a Molecular weight obtained by SEC analysis in THF using PS standards. ^b Dispersity (D_M) obtained by SEC analysis in THF using PS standards. ^c Onset temperature of the thermoresponsive transition.

A key element of our design was to ensure the stability of these micelles, both during *in vitro* and *in vivo* evaluation. To this end, we incorporated sulfhydryl units within the polymer chains to allow for disulfide-mediated crosslinking between polymer chains within the final micellar assemblies. The pentafluorophenyl (PFP) group within the copolymer was subsequently modified to present thiol groups through post-polymerisation modification with cysteamine (CYS).¹⁹ Near quantitative substitution of the pentafluorophenyl groups with CYS to form p(DEGMA-*co*-MACYS) was achieved using the polar aprotic solvent *N,N*-dimethylformamide

1
2
3 (DMF), which is well-known to promote S_N2 substitution reactions.²⁰ This process was
4 monitored through the disappearance of the fluorine peaks (-151.7, -152.7 (ortho), -158.2
5 (para), and -163.3 (meta) ppm) in the ^{19}F NMR spectrum of the polymer (Figure 2C) following
6 amidation. Successful coupling of CYS to the polymer was also observed indirectly, with a
7 significant change in the polymer LCST following modification (Table 1). The LCST onset
8 temperature shifted from 10 °C to 16 °C upon CYS modification (Figure S2), presumably due
9 to modulation of the overall copolymer hydrophobicity through replacement of the PFP group
10 with the more hydrophilic thiol. Moreover, these thiol groups present potential crosslinking
11 sites initiated through disulfide formation that would exhibit redox responsiveness for
12 downstream application of these nanomaterials in drug delivery.²¹

13
14
15
16
17
18
19
20
21
22
23
24
25
26 The final step in the preparation of the responsive hydrophobic component of the amphiphile
27 was chain-end modification to facilitate rapid conjugation of either the biological entity or PEG
28 hydrophile, followed by incorporation of a fluorescent dye (Cy5 maleimide) for tracking
29 purposes. The DBCO-p(DEGMA-*co*-MACYS) copolymer were conveniently prepared
30 through amidation with a heterobifunctional linker (Figure 2).²² Successful modification was
31 monitored by UV-Vis spectroscopy with the appearance of the characteristic absorbance peak
32 of DBCO at 309 nm (Figure 2D) and ^1H NMR which showed the presence of aromatic peaks
33 between 7.3 – 7.65 ppm assigned to DBCO (Figure S1).
34
35
36
37
38
39
40
41
42
43
44
45
46
47
48
49
50
51
52
53
54
55
56
57
58
59
60

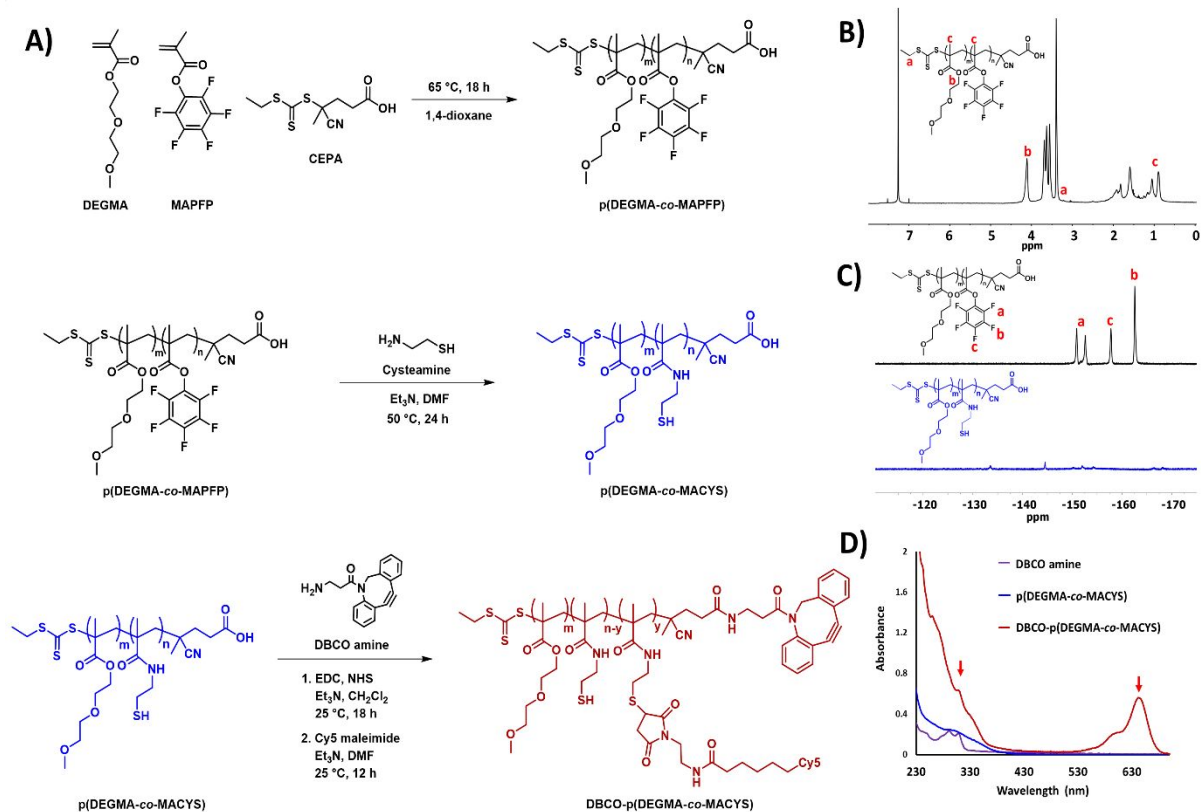


Figure 2. (A) Reaction scheme showing the synthesis of the thermoresponsive, crosslinkable polymer chain for the hydrophobic component of the amphiphiles (B) ¹H NMR (500 MHz, CDCl₃) spectrum of p(DEGMA-co-MAPFP) with (a) methylene protons adjacent to the trithiocarbonate, (b) (DEGMA) side-chain protons, and (c) p(MAPFP) and p(DEGMA) methyl protons. (C) ¹⁹F NMR (470 MHz, CDCl₃) spectra of p(DEGMA-co-MAPFP) copolymer exhibiting the ortho-, meta-, and para- signals associated with the PFP repeat units (black), and after reaction of the polymer with CYS resulting in p(DEGMA-co-MACYS) copolymer (blue) indicating almost complete success of the amidation reaction. (D) UV-Vis spectra in methanol of DBCO amine (purple), p(DEGMA-co-MACYS) (blue) and DBCO-p(DEGMA-co-MACYS) (red) showing the incorporation of DBCO and Cy5 peaks at 309 and 647 nm respectively.

1
2
3 This was followed by conjugation of Cy5 maleimide dye onto a small portion of the thiol
4 groups in the polymer to provide a diagnostic handle for the hydrophobic block, and the
5 subsequent product was characterised using UV-Vis spectroscopy, which showed the
6 characteristic absorbance peak of Cy5 at 647 nm. The LCST of the resulting polymer system
7 was evaluated and shown to be 16 °C, suggesting that successful protein conjugation could
8 occur at temperatures below this point when the polymer was soluble in water, but subsequent
9 heating above this point would lead to self-assembly of the polymer chains (Figure S2). Table
10 1 summarises the physicochemical properties of the hydrophobic component after subsequent
11 modifications.
12
13
14
15
16
17
18
19
20
21
22

23
24 **Development of amphiphilic conjugates.** The thermoresponsive “hydrophobic” polymer
25 described above was then coupled with either scFv-N₃ or PEG-N₃ hydrophiles through SPAAC
26 reaction, a fast catalyst-free click chemistry method, as a convenient route to creating
27 amphiphilic block copolymers.¹⁸ As a model antibody system, an scFv (25 kDa) of the
28 established Prostate-Specific Membrane Antigen (PSMA) targeting antibody, J591, was
29 engineered and produced in bacteria.²³ Moreover, an unnatural amino acid containing azide
30 functionality was engineered into the N-terminus of the scFv to allow convenient azide-alkyne
31 click reactions to occur.²⁴ The scFv was subsequently conjugated to DBCO-p(DEGMA-*co*-
32 MACYS) by incubation in PBS at 4 °C for 24 h resulting in the formation of hybrid conjugates
33 (scFv-p(DEGMA-*co*-MACYS)). After conjugation, these amphiphiles were kept at 30 °C for
34 10 min, leading to insolubility of the thermoresponsive chain. Subsequent centrifugation
35 (14,100 rcf for 10 min) led to precipitation and formation of a hybrid conjugate pellet, while
36 unbound scFvs remained in the supernatant and could be removed. The pellet was then
37 redispersed into PBS and centrifuged with Amicon® Spin filters (MWCO: 30 kDa) to remove
38 any unbound polymer from the hybrid conjugate. The resulting hybrid conjugates were
39
40
41
42
43
44
45
46
47
48
49
50
51
52
53
54
55
56
57
58
59
60

evaluated using HPLC analysis (Figure 3C), and the obtained result is consistent with successful antibody conjugation to the synthetic hydrophobe.²⁵ Successful conjugation was further validated using sodium dodecyl sulfate-polyacrylamide gel electrophoresis (SDS-PAGE) analysis (Figure S3), where the archetypical smearing of the conjugate (lane 4), rather than single sharp band as observed for the scFv alone (lane 2), was indicative of scFv coupling to the synthetic copolymer. The elongated and “smeared” peak was present in SDS PAGE for both Coomassie blue and Cy5 channels (labelling of both the protein and the polymer hydrophobe), further corroborating successful coupling.^{26,27}

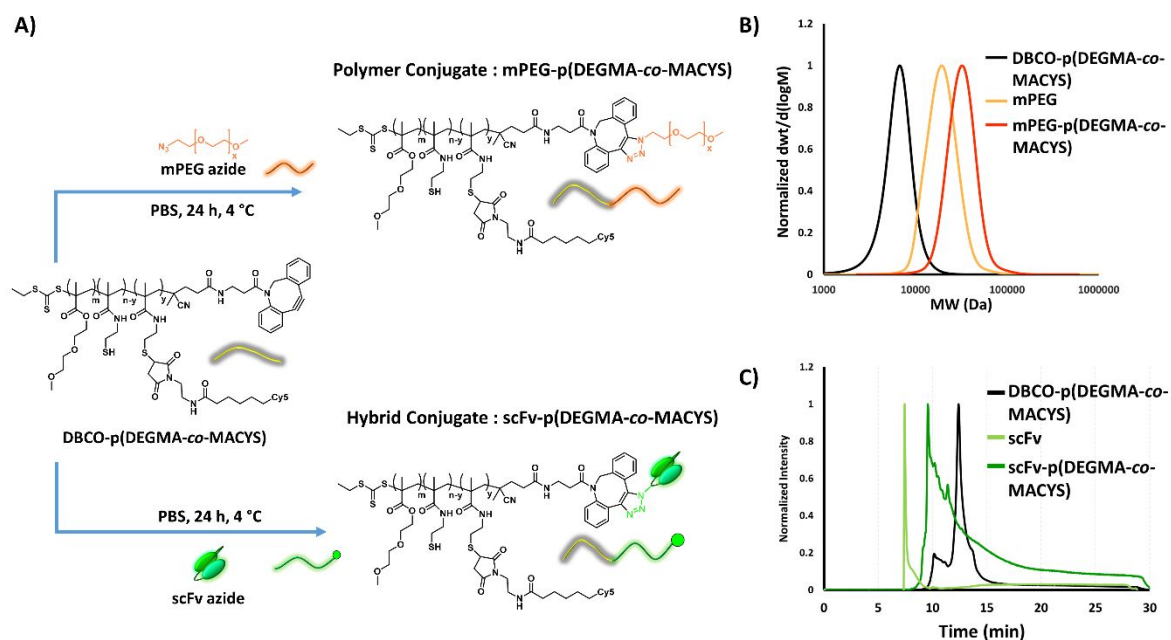


Figure 3. (A) Schematic representation of the structures of both the mPEG and scFv hybrid conjugates. (B) SEC chromatogram of the mPEG-polymer conjugate (red) along with starting materials, mPEG-N₃ (orange) and DBCO-p(DEGMA-co-MACYS) polymer (black). (C) HPLC chromatogram of the hybrid conjugate (dark green) along with controls, J591 scFv-N₃ (light green) and DBCO-p(DEGMA-co-MACYS) polymer (black).

A similar procedure was used to develop the polymer conjugate (mPEG-p(DEGMA-co-MACYS)), in which DBCO-p(DEGMA-co-MACYS) was incubated with commercially-

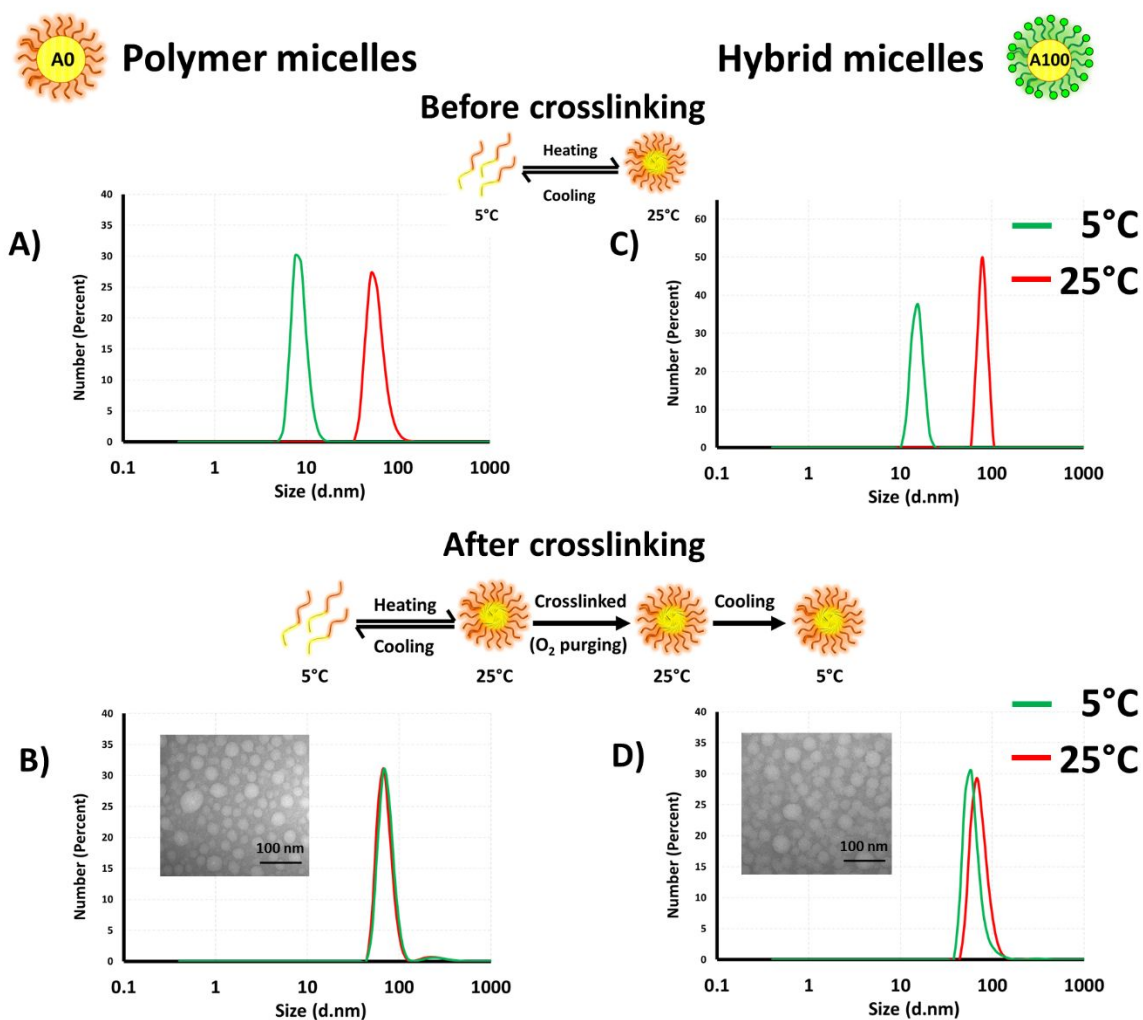
1
2
3 available methoxy-PEG (mPEG) azide in water at 4 °C for 24 h. mPEG has been widely used
4
5 to improve the therapeutic index of clinical drugs,²⁸ and formulations such as mPEG modified
6
7 liposomal doxorubicin (Doxil / Caelyx) are accepted by the Food and Drug Administration
8
9 (FDA) for the treatment of breast cancer.²⁹ In order to prevent recognition by the mononuclear
10
11 phagocytic system (MPS) and thereby impart stealth properties to the micelles, mPEG
12
13 displaying a radius of hydration (R_H) of 4 nm similar to the scFv (Figure S4), was used to form
14
15 mPEG conjugates, with successful coupling demonstrated by size exclusion chromatography
16
17 (Figure 3B).
18
19

20
21 The cellular association of the monomeric conjugates with prostate cancer cells that had high
22
23 (PC3-PIP cells: PSMA+) and low (PC3 cells: PSMA-) levels of PSMA expressions were
24
25 assessed to demonstrate targeting ability of the conjugates.³⁰ Flow cytometry analysis of the
26
27 conjugates following incubation at 4 °C (when the chains would be in their soluble form)
28
29 showed significantly higher association for the hybrid conjugates in PSMA+ cells compared to
30
31 the polymer conjugate (Figure S5). Likewise, in the cells that showed low expression of PSMA
32
33 (PSMA-), much lower association was observed for both conjugates, indicating that the
34
35 mechanism of association was likely *via* receptor-mediated interactions. Importantly, this
36
37 preliminary *in vitro* study suggested that the coupling approach still facilitated successful
38
39 presentation of the scFv for binding to the receptor.
40
41
42
43

44
45 **Synthesis of micellar assemblies.** Micelles were synthesised with varying antibody densities
46
47 by mixing the amphiphilic hybrid conjugates with the polymer conjugates in PBS at
48
49 temperatures below the LCST (16 °C), then increasing the temperature above the LCST,
50
51 whereupon the thermoresponsive behaviour of the hydrophobic component led to self-
52
53 assembly of the conjugates.³¹ This process is reversible, and as an example for purely polymer
54
55 conjugates or hybrid conjugates, Figure 4 shows the size by dynamic light scattering (DLS) of
56
57
58
59
60

1
2
3 unimers (at 5 °C), their assembly into micelles at 25 °C, then subsequent destabilisation and
4
5
6
7
8
9
10
11
12
13
14
15
16
17
18
19
20
21
22
23
24
25
26
27
28
29
30
31
32
33
34
35
36
37
38
39
40
41
42
43
44
45
46
47
48
49
50
51
52
53
54
55
56
57
58
59
60

existence of unimers when cooled back down to 5 °C. Importantly, this process was observed to occur for both the polymer and hybrid conjugates, with the size of the micelles being approximately 70 nm at 25 °C, irrespective of the hydrophile that was used, allowing for a decoupling of micelle size and composition; this was an important pre-requisite for future comparisons (Figure S6). In addition, the zeta potential of the micelles was found to be less affected by an increase in antibody density, with the overall charge remaining neutral independent of antibody density (Figure S7).



1
2
3 **Figure 4.** DLS size distribution of the micelles from polymer conjugate and hybrid conjugates.
4
5 (A) non-crosslinked polymer micelles, (B) crosslinked polymer micelles by oxygen purging,
6
7 (C) non-crosslinked hybrid micelles, and (D) crosslinked hybrid micelles at 25 °C (red) and 5
8
9 °C (green). The insert in 4B and 4D shows the TEM images of crosslinked micelles from
10
11 polymer and hybrid conjugates respectively, indicating an average size of 70 nm. Oxygen
12
13 purging results in crosslinking due to the formation of disulfide bonds between the thiol groups
14
15 of the CYS side-chains.
16
17
18
19

20 The micelles were synthesised by mixing the PEG and hybrid conjugates in varying ratios. In
21
22 order to characterise the amount of antibody components in micelles, a secondary system was
23
24 developed, in which the hybrid conjugates were labelled with Cy5 and the polymer conjugates
25
26 were labelled with RhodamineB (Figure S8). The average PEG-antibody ratios for each system
27
28 were calculated based on the relative fluorescence intensity of Cy5 (for antibody amphiphile)
29
30 to RhodamineB (for polymer amphiphile) (Figure S9). The “theoretical” correction factor was
31
32 calculated based on the feed ratio of antibody:polymer in the hybrids and was compared to the
33
34 actual fluorescence that we determined using the fluorimeter (for the 4 formulations that had
35
36 the highest fluorescence content, *e.g.* A100, A75, A50, A25) with < 5% difference between
37
38 these two values. This implies that there were little or no quenching arising from intermolecular
39
40 interactions in any of these micelle systems. In order to ensure that the micelles were stable
41
42 under both *in vitro* and *in vivo* conditions, the assemblies were transiently crosslinked using
43
44 disulfide chemistry.³² Crosslinking not only acts to lock in the structure of the low glass
45
46 transition temperature hydrophobe (DEGMA) to prevent dynamic exchange of the individual
47
48 micellar components but also ensures stability following intravenous (I.V.) injection, where
49
50 this has been shown to significantly affect *in vivo* accumulation and biodistribution of
51
52 nanomedicines.^{33,34} Here, the thiol-functional group in CYS acts as the crosslinking point by
53
54
55
56
57
58
59
60

1
2
3 forming disulfide bonds by oxidation through oxygen purging.^{35,36} Evaluation of the size of the
4 micelles following oxidation showed crosslinked micelles retained their size even after
5
6 reducing the temperature to below the LCST, suggesting that the micelles were locked in
7
8 conformation (Figure 4B and 4D). TEM micrographs of both micelles are also shown in Figure
9
10 4 (inset), confirming the size of the assemblies formed. The stability of purely synthetic
11
12 micelles was further analysed in cell culture media containing foetal bovine serum (FBS) as
13
14 pseudo-serum conditions, and the structures maintained integrity and size over 24 h (Figure
15
16 S10). However, longer incubation of these micelles in 50% serum-containing media resulted
17
18 in an increase in micelle size, most likely due to higher serum protein interactions (Figure
19
20 S11). Importantly, there was no evidence of degradation of the micelles through observation of small
21
22 fragments in the DLS. Moreover, fluorescence stability of A0 micelles showed < 15% Cy5
23
24 loss in 50% FBS media for an incubation of 48 h (Figure S12). The crosslinking of the micelles
25
26 offers greater control over the material used for *in vivo* experiments and provides confidence
27
28 that the interactions observed are due to micellar interactions, rather than interactions by
29
30 fragments of the micelles.
31
32

33
34 **Effect of ligand density on cellular association and internalisation.** Micelles of varying
35
36 scFv densities (0, 5, 10, 15, 25, 50, 75, 100% chain ratio relative to the PEG-hydrophile) were
37
38 assembled to investigate the relationship between antibody density and cellular association and
39
40 were labelled as A0, A5, A10, A15, A25, A50, A75, and A100, respectively (Figure 1). These
41
42 micelles were incubated with prostate cancer cell lines that either had high expression of PSMA
43
44 (PSMA+) or low expression (PSMA-) for 1 h prior to evaluation of cell binding by flow
45
46 cytometry.³⁰ Cellular association studies using flow cytometry demonstrated that even with a
47
48 small increase in antibody density, micelles typically showed an increased association with
49
50 PSMA+ cells. For these cells that upregulated PSMA, the cellular association was seen to rise
51
52
53
54
55
56
57
58
59
60

1
2
3 with increasing antibody content until reaching a plateau at 25-50% incorporation of antibody,
4 before decreasing modestly at higher incorporation (Figure 5A). This may be due to the
5 potential for receptor saturation, resulting from the interaction between higher amounts of
6 scFvs with the PSMA receptors on the particular cell line. In addition to receptor saturation,
7 the decrease in nanoparticle association might also be due to the competitive binding between
8 micelles onto the receptors.^{37,38} Compared to 50% antibody micelles, 100% micelles have
9 higher antibody content resulting in higher competition for interacting with the active site of
10 the receptors, thereby hindering the cellular association.³⁹⁻⁴¹ The association with PSMA- cells
11 was low, indicating that specific interaction was negligible with receptors on this cell line. This
12 has been further validated using a competition assay, where the PSMA+ cells exhibited
13 significantly reduced cellular association with the targeted micelles when pre-incubated with
14 free scFv ($10 \mu\text{g mL}^{-1}$), compared to when treated with targeted micelles alone (Figure S13).
15 To better understand the observed trend in receptor binding on PSMA+ cells, a binding assay
16 was conducted to explore the effect of different concentrations of antibody containing micelles
17 (A25 and A100) (Figure S14) on cellular association. Under these conditions, the number of
18 micelles at each concentration were approximately the same for A25 and A100. A100 was
19 found to bind to maximum number of cells (% cell association) at a lower concentration than
20 A25 ($25 \mu\text{g/mL}$ compared to $100 \mu\text{g/mL}$, respectively), potentially due to the avidity effect of
21 these nanoparticles (more antibodies to bind with receptors). And when both A25 and A100
22 showed association with 100% of cells ($100 \mu\text{g/mL}$), the MFI was higher for A25 than A100.
23 This suggests that at high concentrations, more of the nanoparticles with lower antibody density
24 can bind to the cells than those with higher antibody density. Therefore, these changes in
25 cellular association might be due to combination of multiple factors including receptor
26 clustering,⁴² receptor crowding by high antibody density nanoparticles⁴³ or steric crowding of
27
28
29
30
31
32
33
34
35
36
37
38
39
40
41
42
43
44
45
46
47
48
49
50
51
52
53
54
55
56
57
58
59
60

the antibody on the nanoparticles⁴⁴ which ultimately leads to difference in the association levels *in vitro*.^{45,46}

Interaction of a subset of the micelles (A0, A25, and A100) with both PSMA+ and PSMA- cells was evaluated by confocal microscopy in order to assess the effect of antibody on the degree of cell internalisation. The microscopy showed a similar trend to that observed in the flow cytometry, whereby higher uptake is observed for the A25 micelle than either the A0 or A100 micelle, again pointing at a receptor-mediated interaction that is modulated by ligand density (Figure 5B).

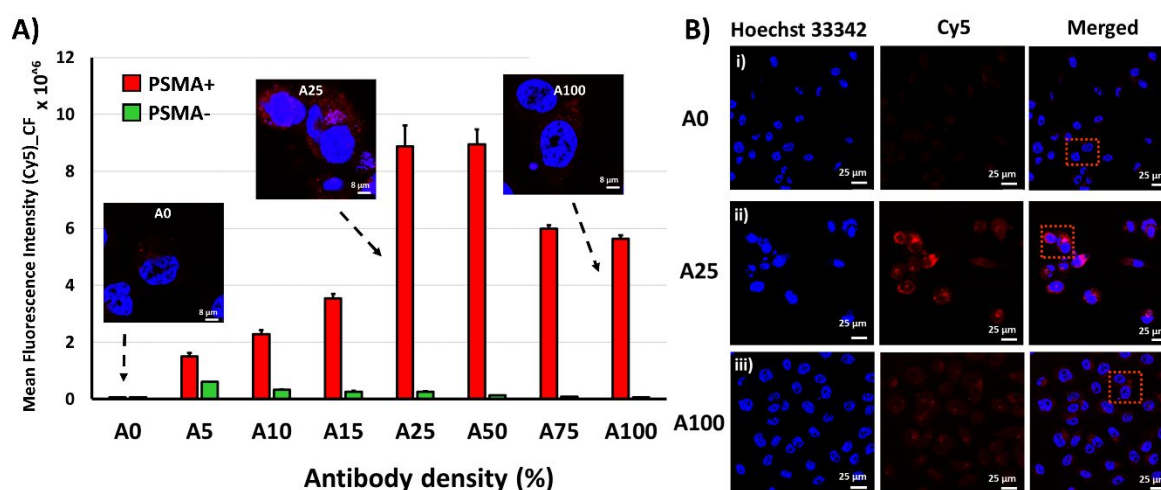


Figure 5. (A) Flow cytometry analysis of PSMA+ and PSMA- cells association of Cy5 labelled micelles with varying antibody densities (0, 5, 10, 15, 25, 50, 75, and 100%). (B) Confocal microscopy images of PSMA+ cells incubated with micelles of varying antibody densities (0, 25 and 100%), along with magnified confocal images showing the distribution of micelles across the PSMA+ cells.

Biodistribution and tumour accumulation of micelles with varying antibody densities in tumour-bearing mice. The influence of ligand density on *in vivo* biodistribution and tumour accumulation was evaluated to understand the balance between increased cell targeting (with increasing ligand density) and tumour accumulation. BALB/c nude mice bearing both

1
2
3 (PSMA+) and (PSMA-) prostate cancer xenografts in their opposite flanks were administered
4 micelles with varying antibody densities through I.V. injection. Mice were sacrificed and organ
5
6 distribution of the Cy5-labelled micelles monitored by fluorescence imaging (24 and 48 h). In
7
8 order to compare the micelles between tumour bearing mice, the fluorescence intensities were
9
10 normalised with respect to the 100% antibody containing micelles, which has been accounted
11
12 for in Table S1. At 24 h post-injection, the PSMA+ tumours demonstrated an antibody-
13
14 dependent micelle accumulation, showing an almost 19-fold increase in micelle accumulation
15
16 with the increase of antibody density from 0% to 25%, owing to enhanced retention in the
17
18 tumour (Figure 6A). However, increasing the antibody content further resulted in a decreasing
19
20 level of tumour accumulation compared to A25, with A50, A75 and A100 micelles only
21
22 achieving a doubling of micelle accumulation compared to A0. This decrease in accumulation
23
24 above A25 was most likely caused by a decreased concentration of circulating micelles due to
25
26 immune recognition of the more proteinaceous nanomaterials. Such an effect ultimately leads
27
28 to the clearance by the mononuclear phagocytic organs such as liver and spleen. This scenario
29
30 was confirmed by the increase in fluorescence in these organs with increasing antibody content
31
32 (Figure 6B), thereby resulting in a decrease in overall circulating micelle content in the blood
33
34 and consequently decreased accumulation in the tumour at longer time points. At 24 h post-
35
36 injection, the PSMA- tumour showed significantly less micelle accumulation in the tumour at
37
38 all antibody compositions and similar to that observed for A0 (in both tumours), suggesting
39
40 that the presence of antibody (even in the A100 sample) contributes to improvement in tumour
41
42 tissue accumulation above that observed by the enhanced permeability and retention (EPR)
43
44 effect alone.⁴⁷
45
46
47
48
49
50
51
52
53
54
55
56
57
58
59
60

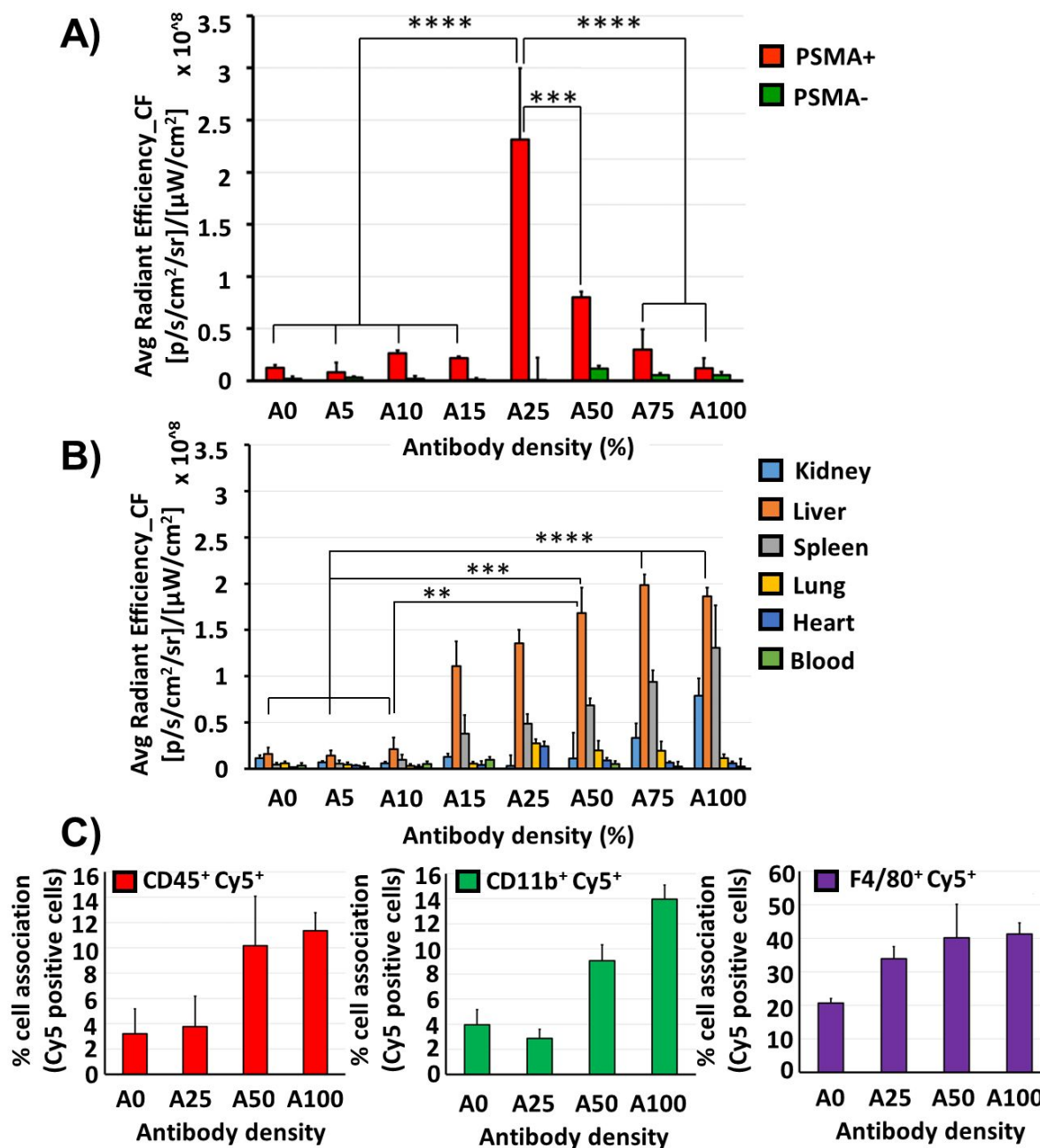


Figure 6. (A) Bar chart showing the average radiant efficiency of Cy5 signals from PSMA+ and PSMA- tumour, 24 h post-I.V. injection of micelles with varying ligand densities of 0, 5, 10, 15, 25, 50, 75, 100% antibody content. (B) Bar chart showing the average radiant efficiency of Cy5 signals from other major organs, 24 h post-I.V. injection of micelles with varying ligand densities of 0, 5, 10, 15, 25, 50, 75, 100% antibody content. (C) Bar chart showing the cellular association of micelles with immune cells such as leukocytes (CD45⁺), monocytes (CD11b⁺)

1
2
3 and macrophages (F4/80⁺) in the liver after 24 h post-I.V. injection of micelles with varying
4 ligand densities of 0, 25, 50, and 100% antibody content. (n = 3 per group), (** = p < 0.01, ***
5 = p < 0.001, **** = p < 0.0001).

6
7
8
9
10
11 A similar trend in accumulation is observed at 48 h, where the effect of passive targeting (to
12 PSMA-) was slightly more prominent than the 24 h time point (Figure S15).

13
14 **Micelle association with murine immune cell populations.** The ratio of PEG to antibody
15 component on the surface of the micelles has a significant impact on its accumulation and
16 distribution across tumour and other organs. It is crucial to understand the influence of antibody
17 density on the interactions between micelles and immune cells, predominantly present in the
18 liver and spleen for nanoparticles. These immune cells constitute the MPS, and upon
19 stimulation results in rapid clearance of micelles from animals. We established a flow
20 cytometric assay to furnish important insights into micelle distribution between different
21 immune cell types in liver and spleen following injection of the micelles into
22 immunocompetent mice (Figure 6C, S16 and S17). The use of a CD45 marker (to identify
23 immune populations from other cell types in the organ), as well as a live/dead exclusion dye,
24 provided a useful means to investigate immune-trafficking of the micellar particles. In terms
25 of gating strategy, after identifying the immune cells (CD45⁺) from the whole cell population,
26 additional markers such as CD11b and F4/80 were used to distinguish monocytes and
27 macrophage subpopulations, respectively. The flow cytometry suggested a 3-fold higher
28 proportion of A100 micelles in whole immune cell (CD45⁺) populations compared to the A0
29 micelles (Figure 6C). The CD11b⁺ cell population includes monocytes, a subset of white blood
30 cells that play a key role in homeostasis and inflammation, and can be readily transported to
31 the site of inflammation.⁴⁸ In the CD11b⁺ cell population in liver and spleen, the association
32 was three- to eight-fold higher for hybrid micelles compared to polymer micelles, with
33
34
35
36
37
38
39
40
41
42
43
44
45
46
47
48
49
50
51
52
53
54
55
56
57
58
59
60

1
2
3 increasing association with greater antibody content. We also observed higher cellular
4 association for F4/80+ macrophages in the case of A100 micelles. Generally, Kupffer cells and
5 splenic red pulp macrophages show high levels of expression for F4/80 glycoprotein and have
6 critical roles in immune surveillance, with Kupffer cells being the major route of nanoparticle
7 removal from circulation.^{49,50} The increased immune response for A100 micelles with an
8 increase in antibody content clearly indicates an active role of the immune system in
9 recognising, and clearing these micelles from circulation. After I.V. injection of micelles,
10 serum proteins in the blood binds to these micelles resulting in a protein corona.⁵¹⁻⁵⁴ This
11 binding depends on the surface properties of the micelles; for instance, PEGylation blocks the
12 serum protein interaction resulting in lower MPS recognition. However, the presence of
13 antibodies on the micelle surface triggers the serum protein interaction and thereby results in
14 enhanced liver and spleen clearance. To exemplify this point, interactions between micelles
15 and serum proteins were studied by incubating them in FBS containing cell culture media. In
16 this experiment, the serum protein interaction was significant only for an antibody content of
17 50% or higher (Figure S18) in the micelles. Furthermore, an evaluation of the micelle
18 distribution in various immune cells in mice blood *ex vivo* was also carried out. In general, the
19 higher the antibody content in the micelle, the greater the interaction with all elements of the
20 immune cell populations that we investigated. Moreover, more specific association with blood
21 immune cell populations, including neutrophils and monocytes, was observed at higher
22 antibody concentrations (Figure S19).

23
24
25
26
27
28
29
30
31
32
33
34
35
36
37
38
39
40
41
42
43
44
45
46
47
48
49 **Micelle accumulation in human white blood cells.** A key issue in the translation of
50 nanomedicines to clinical acceptance is the mismatch between observations in mouse and
51 human studies. With this in mind, we next investigated the micellar association with the
52 immune population of cells in whole human blood, as these will be the first host cells that
53
54
55
56
57
58
59
60

1
2
3 interact with micelles following I.V. administration.⁵⁵ Human blood immune cells such as
4 granulocytes (mainly neutrophils), monocytes, lymphocytes (B-cell and T cell) and dendritic
5 cells were analysed after incubation with the micelles with fresh whole human blood for 1 h at
6 37 °C using established methodologies previously reported by Kent *et al.*⁵⁶ Overall, there was
7 a clear modulation in immune-cell interaction as a result of increasing antibody content in the
8 micelles. Association was highest for A100 and A75 micelles with granulocytes, with
9 approximately 80-90% cells showing some interaction with the micelles (Figure 7A). While
10 A50 micelles showed 40% association, further lowering of antibody content showed minimal
11 association. This observation clearly shows immune recognition resulting from the interaction
12 of antibody component with neutrophils and its phagocytic nature.⁵⁵ Within the monocyte
13 population, A0 micelles showed less than 1% cellular association indicating its stealth nature,
14 a direct consequence of the purely PEG surface nature of this particular micelle. However, 10%
15 or higher antibody content showed an increase in cellular association with >10% of cells
16 showing a measurable association when the antibody component of the micelles was 50%
17 (Figure 7B). Similar trends were observed for both lymphocyte populations and dendritic cells
18 (gating strategy used for differentiating cell populations are shown in Figure S20). These
19 results showed a direct link between the level of antibody density and immune-cell interaction,
20 with an enhanced immune clearance of the micelles with $\geq 50\%$ antibody content. These human
21 *ex vivo* blood studies are precisely comparable to our *in vivo* mouse studies above, suggesting
22 that the findings are likely to be transferable (at least in the broadest sense) to clinical
23 assessment of nanomedicines. More importantly, these in-depth immune studies offer some
24 important insight into why greater antibody density often leads to a mismatch between *in vitro*
25 cancer cell association studies (undertaken extensively *in vitro* in nanomedicine research) and
26 tumour accumulation and/or efficacy studies of nanotherapeutics.⁹ It is clear that each
27
28
29
30
31
32
33
34
35
36
37
38
39
40
41
42
43
44
45
46
47
48
49
50
51
52
53
54
55
56
57
58
59
60

1
2
3 nanomedicine needs to be assessed on a case-by-case basis, where the merit of targeting
4 specific receptors present on cells is weighed against the need for stealthiness.
5
6

7
8 It is also important to consider the effects of multiple copies of a targeting agent on the cell
9 surface and intracellular processing pathways more generally. Pattern recognition by the
10 immune system is an important mechanism in the body's defence against pathogens,
11 particularly viruses which display multiple ligands in order to take advantage of multivalent
12 interactions. Accordingly, the use of repeating patterns of protein recognition domains on a
13 synthetic nanoparticle might be expected to result in increased detection by immune
14 surveillance mechanisms. In addition, it has been shown that engagement of multiple receptors
15 at some cancer cell surfaces can lead to clustering and changes in intracellular trafficking
16 pathways leading to lysosomal accumulation.^{12,14} This might be detrimental for delivery of
17 biotherapeutics but advantageous for lysosomally-activated pro-drugs. Therefore, it may be the
18 case that an optimal targeting ligand density exists and that this will depend on the route of
19 administration, the immune status of the patient, and the specific disease site and therapeutic
20 agent. The results in this study provide important design criteria which might allow future
21 optimisation and ultimately personalisation of nanomedicines.
22
23
24
25
26
27
28
29
30
31
32
33
34
35
36
37
38
39
40
41
42
43
44
45
46
47
48
49
50
51
52
53
54
55
56
57
58
59
60

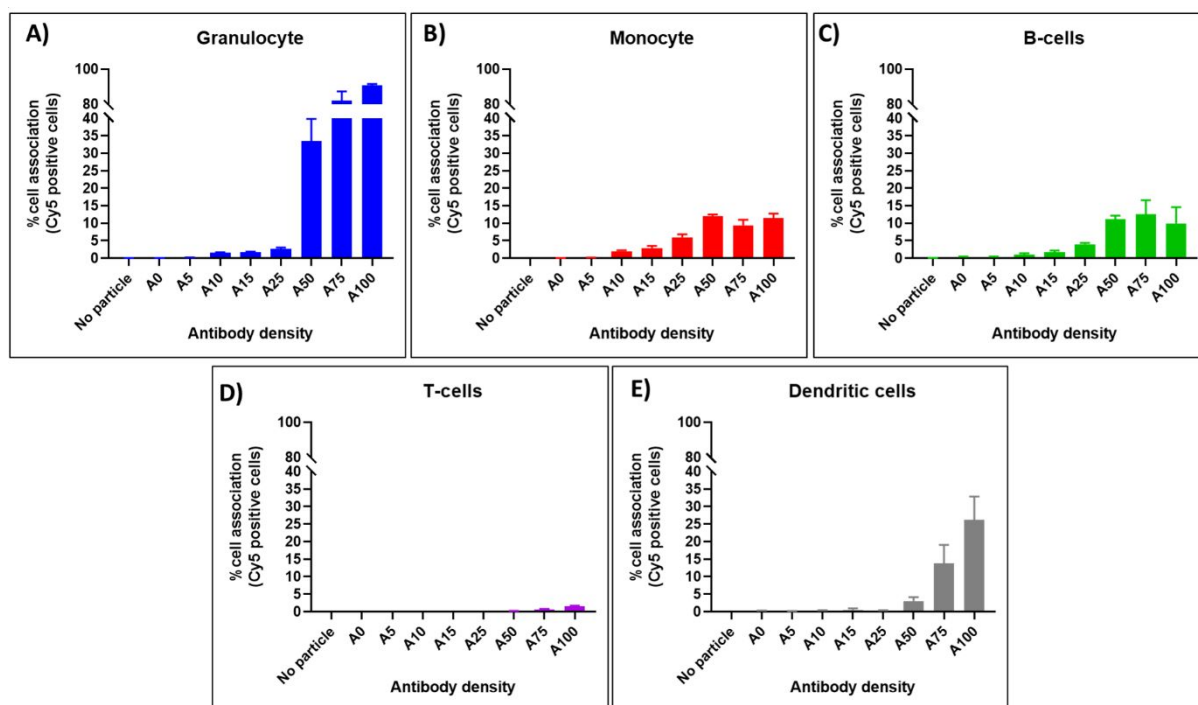


Figure 7. Effect of antibody density on the interaction of micelles with human innate immune cells. Histograms show the percentage cellular association of micelles with (A) Granulocytes, (B) Monocytes, (C) B-cells, (D) T-cells, (E) Dendritic cells at 37 °C.

CONCLUSION

We report an approach to generate a micellar nanomaterial platform with control over antibody fragment surface density, allowing us to study in-depth the true influence of surface functionalisation on both cell binding, immune recognition and tumour accumulation of nanomedicines. The micellar assemblies showed antibody-density dependent association and internalisation in cells that upregulate a receptor that binds to the antibody (PSMA receptor), with maximum association observed between 25 – 50% antibody surface density. The decrease in association at higher densities was attributed to receptor saturation or potentially clustering effects of the receptor on the cell surface. Moreover, when administered intravenously into tumour-bearing mice, significantly enhanced tumour association was observed for the micelle with 25% antibody density compared to all other densities. The decrease in accumulation at a

1
2
3 higher density above 25% was shown to be proportional to the increase in immune recognition
4
5 of these species and subsequent clearance through the MPS organs. The micelles clearly
6
7 become less “stealthy” in mice with greater antibody content, which was also confirmed by our
8
9 *ex vivo* human whole blood analyses. Additionally, our studies on human white blood cells
10
11 demonstrated that the higher antibody densities had an influence on immune cell interactions.
12
13 These results provide an understanding of how these fundamental properties of designed
14
15 nanoparticles can be utilised to enhance cellular uptake, and influence biodistribution in
16
17 animals, and later into clinical settings. Moreover, it is clear that there is at least a broad level
18
19 of agreement between mouse immune studies and the human case, suggesting translatability of
20
21 these observations when designing nanomedicines for human use. In the cancer nanomedicine
22
23 field, it is becoming increasingly clear that just delivering the payload to the target is not
24
25 enough but now requires an in-depth understanding of the collateral damage these
26
27 nanomaterials could have to healthy immune cells. Ultimately, accessing the “sweet spot” in
28
29 terms of increasing cell-association/internalisation through increased antibody density (often a
30
31 necessity for delivery of specific drugs, such as biologics), and minimising immune recognition
32
33 by maintaining stealthiness, are now key attributes for developing next-generation targeted
34
35 nanomedicines that could offer improved clinical outcomes.
36
37
38
39
40
41
42
43
44

45 **EXPERIMENTAL**

46 **Materials**

47
48 Dibenzocyclooctyne-amine (DBCO, Sigma-Aldrich, $\geq 94.5\%$), triethylamine (Et_3N , Sigma-
49
50 Aldrich, $\geq 99\%$), 2,2'-azobis(isobutyronitrile) (AIBN, Sigma-Aldrich, 98%), 1-ethyl-3-(3-
51
52 dimethylaminopropyl) carbodiimide hydrochloride (EDC, Fluorochem, 99%), *N*-
53
54 hydroxysuccinimide (NHS, Sigma-Aldrich, 98%), cysteamine hydrochloride (CYS, Sigma-
55
56
57
58
59
60

1
2
3 Aldrich, $\geq 98\%$), methoxy-PEG-azide ($M_n=20$ kDa) (mPEG, Biochempeg, $\geq 95\%$), Cyanine5
4 maleimide (Cy5, Lumiprobe, $> 95\%$), phosphate-buffered saline (PBS, Astral scientific) were
5 all used as received. Solvents including *N,N*-dimethyl-formamide (DMF), 1,4-dioxane,
6 methanol, tetrahydrofuran (THF), *n*-hexane, and dichloromethane (CH_2Cl_2) were used dry
7 where applicable and of reagent grade quality. Diethylene glycol methacrylate (DEGMA,
8 Sigma-Aldrich, 98%) were passed through basic alumina to remove inhibitor before use. Milli-
9 Q water ($18.2 \text{ m}\Omega\cdot\text{cm}^{-1}$ at $25 \text{ }^\circ\text{C}$) was used throughout. Pentafluorophenyl methacrylate
10 (MAPFP) was synthesised according to Fuchs *et al.*⁵⁷ RAFT agent 4-Cyano-4-
11 (ethylsulfanylthiocarbonyl) sulfanylpentanoic acid (CEPA) was synthesised according to
12 Convertine *et al.*⁵⁸ Dimethyl sulfoxide- d_6 (DMSO- d_6), deuterated chloroform (CDCl_3) were
13 purchased from Cambridge Isotope Laboratories, Inc. Cell culture medium Roswell Park
14 Memorial Institute (RPMI) 1640, foetal bovine serum (FBS), were purchased from Life
15 Technologies, Mulgrave, Vic, Australia and Moregate, Brisbane, Australia respectively.
16 Penicillin/streptomycin mix, trypsin, trypan blue solution and Hoescht 33342 were obtained
17 from Sigma-Aldrich. Prostate cancer cells (PC3-PIP (PSMA+) and PC3 (PSMA-) cells were
18 received from Dr Warren Heston.⁵⁹ Tissue culture treated imaging μ -dishes with 1.5 NA
19 coverslips were ordered from ibidi™.

42 **Methods**

43
44 All nanomaterials were characterised using standardised reporting methods recommended by Faria
45 *et al.*, where applicable.⁶⁰ ^1H nuclear magnetic resonance (NMR), ^{19}F NMR spectra were
46 measured on Bruker AC 400 or 500 MHz spectrometers in CDCl_3 or DMSO- d_6 at $25 \text{ }^\circ\text{C}$.

47
48
49
50
51 are reported as δ in parts per million (ppm) and referenced to the chemical shift of

52
53
54 the residual solvent resonances (CDCl_3 ^1H : $\delta = 7.26$ ppm; DMSO- d_6 ^1H : $\delta = 2.50$ ppm).

1
2
3 Size exclusion chromatography (SEC) for analysis of polymer molecular weight and dispersity
4 was performed on a system consisting of a 1515 Isocratic pump (Waters), a 717 autosampler
5 (Waters), Styragel HT 6E and Styragel HT 3 columns (Waters), a 2414 differential refractive
6 index detector (Waters). THF was used as the mobile phase at a flow rate of 1 mL min⁻¹ and
7 polystyrene (PS) as the standards. Empower 2 (Waters) software was used for data collection
8 and processing. All samples were freshly prepared before analysis and filtered through a 0.45
9 µm filter to eliminate large particulates. The hydrodynamic diameters and zeta potentials of
10 micelles were explored on a Nanoseries Zetasizer (Malvern 90, UK). The samples were
11 analysed at a scattering angle of 90° and two different temperatures 278 and 298 K,
12 respectively. Samples were filtered through 0.45 µm PTFE filters prior to measurement. UV-
13 Vis measurements were performed on a Nanodrop 2000C spectrophotometer (Thermo Scientific)
14 using a low volume (700 µL) quartz cuvette with a 10 mm path length. Absorbance maxima were
15 recorded at 309 and 647 nm for DBCO and Cy5 absorbance respectively. For transmission electron
16 microscope (TEM) imaging, particles were dissolved in water, dropped onto copper grids, and
17 air-dried before imaging. Polyacrylamide gel electrophoresis (PAGE) was performed on
18 Bolt™ 4-12% Bis-Tris Plus Gels (Invitrogen, Paisley, UK) equipped with a PowerPac Basic
19 power supply at 200 V for 30 min in 1X NuPAGE® MES SDS Running Buffer . The
20 visualisation of the Coomassie blue-stained gels was carried out on a ChemiDoc Imaging
21 system, Bio-Rad. High-performance liquid chromatography (HPLC) was performed on Dionex
22 HPLC-Thermo TSQ Quantum Ultra QqQ MS couple equipped with UV-visible detector and a
23 reverse-phase C₁₈ column (75 × 4.6 mm). Gradient elution from 95% Milli-Q water containing
24 0.2% formic acid to 100% MeCN:H₂O (8:2) with 0.2% formic acid over a time period of 30
25 min with a 200 µL min⁻¹ flow rate was used throughout. The wavelengths of 280 nm and 647
26 nm were used for the detection of antibody and conjugates respectively for the analysis.
27
28
29
30
31
32
33
34
35
36
37
38
39
40
41
42
43
44
45
46
47
48
49
50
51
52
53
54
55
56
57
58
59
60

1
2
3 **Cell culture.** Two human prostate cancer cell lines (PC3-PIP (PSMA+) and PC3 (PSMA-))
4 were maintained in RPMI medium supplemented with 10% (v/v) FBS (heat-inactivated,
5 Bovogen), 100 U mL⁻¹ penicillin, 100 µg mL⁻¹ Streptomycin and 2 mM L-glutamine and
6 incubated at 37 °C in a humidified atmosphere of 5% CO₂ in air.
7
8
9

10
11
12 **Synthesis of p(DEGMA-co-MAPFP) copolymer using CEPA.** DEGMA (0.3 g, 1.59 mmol),
13 MAPFP (45 mg, 0.18 mmol), AIBN (1.1 mg, 6.89 × 10⁻³ mmol), CEPA (9.1 mg, 3.44 × 10⁻²
14 mmol) and 660 µL dry 1,4-dioxane were placed in a Schlenk tube equipped with a magnetic
15 stirrer bar. The vial was sealed with a rubber septum, and the reaction mixture was sparged
16 with nitrogen for 15 min. The Schlenk tube was then placed in an oil bath and stirred at 65 °C
17 for 18 h. At the completion of the reaction, the polymer was precipitated dropwise into an
18 excess of *n*-hexane three times. Once the polymer had fully settled on the bottom of the beaker,
19 the solvent was decanted from the top, and the oily residue was dried in the vacuum oven. The
20 purified p(DEGMA-co-MAPFP) was characterised using ¹H NMR (500 MHz, CDCl₃) and
21 SEC.
22
23
24
25
26
27
28
29
30
31
32
33

34
35 **Modification of p(DEGMA-co-MAPFP) copolymer with CYS.** The pentafluorophenyl
36 esters were replaced by adding 20 eq. of CYS (46 mg, 0.454 µM) and 20 eq. of Et₃N (35 mg,
37 0.45 µM) to p(DEGMA-co-MAPFP) copolymer (150 mg, 0.022 µM) dissolved in DMF. The
38 solution was stirred at 50 °C for 24 h. The reaction was cooled to room temperature, and DMF
39 was removed *in vacuo*. The concentrated sample was redissolved in THF and purified by
40 precipitating the polymer dropwise into an excess of *n*-hexane. The purified p(DEGMA-co-
41 MACYS) was dried under vacuum for 24 h. These polymers were characterised using ¹⁹F NMR
42 (500 MHz, CDCl₃) and SEC. The LCST behaviour of polymer samples after CYS modification
43 were determined using a UV-vis spectrophotometer set at 500 nm. The polymeric samples
44 were maintained at a concentration of 1 mg mL⁻¹ in water and the solutions were heated from
45
46
47
48
49
50
51
52
53
54
55
56
57
58
59
60

1
2
3 low temperatures to high temperatures at a heating rate of 1 °C min⁻¹. The temperature at which
4
5 90% of the transmittance of the solution was observed was defined as the LCST.
6
7

8 **Modification p(DEGMA-*co*-MACYS) copolymer with DBCO-amine.** p(DEGMA-*co*-
9
10 MACYS) copolymer (150 mg, 27.5 μM) was activated by NHS (3.5 mg, 30 μM) and EDC
11
12 (10.5 mg, 55 μM) (molar ratio of Polymer: EDC: NHS=1:2:1.1) in CH₂Cl₂ at room temperature
13
14 overnight. DBCO-amine (7.6 mg, 27.5 μM) with Et₃N (3 mg, 30.3 μM) was added and stirred
15
16 for 12 h. DCM was removed by rotary evaporation at room temperature, and the product
17
18 DBCO-p(DEGMA-*co*-MACYS) was redissolved in THF and precipitated into *n*-hexane. The
19
20 purified DBCO-p(DEGMA-*co*-MACYS) was dried under vacuum for 24 h and characterised
21
22 using ¹H NMR (500 MHz, DMSO-*d*₆), SEC and UV analysis
23
24
25

26 **Conjugation of DBCO-p(DEGMA-*co*-MACYS) with Cy5 maleimide.** DBCO-p(DEGMA-
27
28 *co*-MACYS) copolymer (150 mg, 21.7 μM) was reacted with Cy5 maleimide (1.4 mg, 2.17
29
30 μM) in CH₂Cl₂ at room temperature for 12 h. DCM was removed by rotary evaporation at
31
32 room temperature, and the product was redissolved in THF and precipitated into *n*-hexane. The
33
34 purified DBCO-p(DEGMA-*co*-MACYS) with Cy5 maleimide was dried under vacuum for 24
35
36 h and characterised using UV analysis.
37
38
39

40 **Conjugation of DBCO-p(DEGMA-*co*-MACYS) with scFv azide.** Before the conjugation
41
42 reaction, DBCO-p(DEGMA-*co*-MACYS) copolymer was dissolved in PBS and kept for
43
44 stirring at 4 °C for 1 h. Then, the azide-functional scFv was added to the DBCO-p(DEGMA-
45
46 *co*-MACYS) copolymer solution, and the mixture was allowed to react at 4 °C for 24 h. For a
47
48 typical preparation, 5 mg of DBCO-p(DEGMA-*co*-MACYS) copolymer (0.72 μmol) and 0.89
49
50 μg of scFv (3.5 × 10⁻² μmol) were used (Polymer to scFv azide ratio of ~ 20:1). After
51
52 conjugation, samples were heated to temperature above LCST, 30 °C for 10 min, which made
53
54 the polymer insoluble. Upon centrifugation (14,100 rcf for 10 min) the hybrid conjugate formed
55
56
57
58
59
60

1
2
3 a pellet, and unreacted scFv remained in the supernatant. This pellet was redissolved in PBS at
4
5 4 °C and centrifuged at 9,800 rcf for 10 min using Amicon® Ultra 0.5 mL Centrifugal Filters
6
7 (MWCO: 30 kDa) to remove any unbound polymer from the hybrid conjugate. The final
8
9 concentrate was freeze-dried and re-dissolved for further characterisation using PAGE and
10
11 HPLC analysis.
12

13
14 **Conjugation of DBCO-p(DEGMA-*co*-MACYS) with mPEG azide.** For the synthesis of
15
16 polymer conjugate, the DBCO-p(DEGMA-*co*-MACYS) copolymer was dissolved in PBS and
17
18 kept stirring at 4 °C for 1 h. Then, mPEG-azide was added to the DBCO-p(DEGMA-*co*-
19
20 MACYS) copolymer solution, and the mixture was allowed to react at 4 °C for 24 h. For a
21
22 typical preparation, 4.1 mg of DBCO-p(DEGMA-*co*-MACYS) copolymer (0.6×10^{-6} mol),
23
24 and 6 mg of mPEG-azide (0.3×10^{-6} mol) were used (Polymer to mPEG azide ~ 2:1). After
25
26 conjugation, samples were heated to temperature above LCST, 30 °C for 10 min, which made
27
28 the polymer insoluble. Upon centrifugation (14,100 rcf for 10 min), the polymer conjugate
29
30 formed a pellet, and unreacted PEG remained in the supernatant, which could be removed. This
31
32 pellet was redissolved in PBS at 4 °C and centrifuged at 9,800 rcf for 10 min using Amicon®
33
34 Ultra 0.5 mL Centrifugal Filters (MWCO: 30 kDa) to remove any unbound polymer from the
35
36 polymer conjugate. The final concentrate was freeze-dried and re-dissolved for further
37
38 characterisation using SEC analysis.
39
40
41
42
43

44 **Flow cytometry-based cellular association analysis of conjugates using a mono cell**
45
46 **culture.** PSMA+ cells were removed from tissue culture flasks by adding trypsin and
47
48 resuspended in Dulbecco's PBS (DPBS) at pH 7.4 followed by centrifugation at 131 rcf for 5
49
50 min. The cell pellet was resuspended in 10% FCS-PBS to give 2×10^6 cells/mL. 100 μ L of the
51
52 cell suspension was aliquoted into 1.5 mL tubes and stored on ice. 10 μ g mL⁻¹ of hybrid
53
54 conjugate and PEG conjugate were added to the 100 μ L cell suspension and incubated for 60
55
56
57
58
59
60

1
2
3 min on ice. Following incubation, the cells were centrifuged gently at 131 rcf for 5 min, the
4 supernatant was pipetted off and 200 μL of 10% FCS-PBS added. This wash step was repeated
5
6 two more times. After the third and final wash, the supernatant was removed from the cells,
7
8 and the pellet was resuspended in 100 μL of 10% FCS-PBS. For each sample, data were
9
10 acquired for 10,000 events using a flow cytometer (BD Accuri™ C6, BD Biosciences,
11
12 Australia) by measuring Cy5 fluorescence intensity along with the forward and side scatter. A
13
14 similar protocol was used for the analysis of PSMA- cells.
15
16
17
18
19

20 **Synthesis of polymeric micelles by crosslinking and its characterisation.** The hybrid and
21
22 PEG conjugates were dissolved in different ratios in PBS and kept for stirring at 4 °C for 2 h.
23
24 The solution temperature was then increased slowly to 30 °C under constant stirring. Oxygen
25
26 was sparged into the solution for 12 h to facilitate disulfide crosslinking. Micelle confirmation
27
28 and size were then determined by DLS and TEM. The zeta potential distribution of the micelles
29
30 were determined using Zetasizer. Micelles of different antibody densities (0, 5, 10, 15, 25, 50,
31
32 75 and 100%) were synthesised by a similar protocol.
33
34
35

36 **Interaction of micelles with serum proteins.** For serum protein-micelle interaction studies,
37
38 100 μL of 1 mg mL^{-1} micelles were incubated with 400 μL of cell culture media (containing
39
40 10% FBS) for 1 h incubation at 37 °C. Samples were then centrifuged at 14,100 rcf for 4 min,
41
42 to pellet the protein-bound micelles. The amount of unbound serum protein remaining in the
43
44 supernatant was then measured by the method of Bradford assay. Briefly, 100 μL of supernatant
45
46 was taken in triplicate aliquots, and 100 μL of Bradford reagent was added. Samples were
47
48 mixed and incubated at 37 °C for 30 min, followed by measurement of absorbance at 595 nm.
49
50 The absorbance values were normalised against the control sample.
51
52
53

54 **Stability analysis of micelles with 50% serum proteins.** For the stability analysis of micelles,
55
56 500 μL of 1 mg mL^{-1} micelles were incubated with 1500 μL of cell culture media (containing
57
58
59
60

1
2
3 50% FBS) for 48 h incubation at 37 °C. Samples were then analysed using DLS for size and
4 stability assessments. 100 µL of A0 sample (0.5 mg mL⁻¹) was taken in 96 well plate, 100 µL
5 of cell culture media (containing 50% FBS) were added and incubated for 48 h at 37 °C.
6
7 Samples were then analysed using IVIS Lumina X5 imaging system (PerkinElmer Inc.,
8 Waltham, MA, USA) and analyzed using the Living Image software (PerkinElmer Inc.). The
9
10 620_{Ex}/670_{Em} was used to analyze Cy5 fluorescence by micelles. Furthermore, A25 and A100
11
12 micelles were incubated in 50% serum containing media for 48 h, followed by centrifugation
13
14 at 9,800 rcf for 10 min using Amicon® Ultra 0.5 mL Centrifugal Filters (MWCO: 3 kDa). The
15
16 amount of Cy5 dye content in the sample was analysed at 647 nm using UV analysis.
17
18
19
20
21
22

23 **Flow cytometry-based cellular association analysis of micelles using a mono cell culture.**

24 PSMA+ cells were seeded in a 12-well plate at a concentration of 5 × 10⁴ cells mL⁻¹ and then
25
26 incubated in 1 mL of RPMI media for 24 h to allow cells to adhere. Cellular association of the
27
28 micelles into cells was then measured using flow cytometry after 1 h of exposure to 10 µg mL⁻¹
29
30 of micelles of varying antibody densities (0, 5, 10, 15, 25, 50, 75 and 100%). Cells were
31
32 removed from culture dishes by addition of trypsin and resuspended in Dulbecco's PBS
33
34 (DPBS) at pH 7.4 followed by centrifugation at 131 r.c.f. for 5 min. The supernatant was then
35
36 removed, and cells were resuspended in 1 mL of DPBS. For each sample, data were acquired
37
38 for 10,000 events using a flow cytometer (BD Accuri™ C6, BD Biosciences, Australia) by
39
40 measuring Cy5 fluorescence intensity along with the forward and side scatter. A similar
41
42 protocol was used for the analysis of PSMA- cells. Furthermore, for competition assay,
43
44 PSMA+ cells were pretreated with 10 µg mL⁻¹ of J591 scFv for 30 min, following similar
45
46 protocol as mentioned above. Cellular association of the A25 and A100 micelles into PSMA+
47
48 cells were also carried out using flow cytometry after 1 h of exposure to varying concentrations
49
50 of micelles (1 – 100 µg mL⁻¹).
51
52
53
54
55
56
57
58
59
60

1
2
3 **Evaluation of intracellular distribution and localisation of micelles using confocal**
4 **microscopy.** Prior to imaging, PSMA⁺ cells were plated into Ibidi™ μ -dishes and incubated
5
6 with 2 mL of RPMI media overnight. Cells were then exposed to 10 $\mu\text{g mL}^{-1}$ of A0, A25 and
7
8 A100 micelles, incubated for 1 h followed by PBS wash to remove unbound micelles. Samples
9
10 were imaged with an inverted Confocal Laser Scanning Microscope (Leica LASX TCS SP8)
11
12 housed at the Australian Nanofabrication Facility (ANFF). In order to identify the distribution
13
14 of the micelles inside the cells, the nucleus was stained using Hoechst 33342 dye (excitation
15
16 405 nm, emission 416 - 487 nm). The 633 nm laser was used for excitation of the Cy5-labelled
17
18 polymer micelles, and the emission was collected between 645 - 680 nm.
19
20
21
22

23
24 **Animal studies and tumour model.** All animal experiments were approved by the University
25
26 of Queensland's Animal Ethics Committee and conformed to the guidelines of the Australian
27
28 Code of Practice for the Care and Use of Animals for Scientific Purposes. For all animal
29
30 models, eight-week-old Balb/c nude mice were acquired from the Animal Resource Centre and
31
32 were allowed access to food and water *ad libitum* throughout the course of the experiment.
33
34

35 ***In vivo* biodistribution of micelles with varying antibody densities in tumour bearing mice**
36 **using optical imaging.** A total of 50 Balb/c nude mice were used in this study. To establish
37
38 subcutaneous tumours for *in vivo* targeting experiments, mice were anaesthetised using 2%
39
40 isoflurane and injected subcutaneously with 2×10^6 PSMA⁺ cells (left flank) and 2×10^6
41
42 PSMA⁻ cells (right flank), each in 100 μL serum-free media using a 27 G needle. Tumours
43
44 were allowed to grow for 15 days before imaging experiments, at which time all mice had
45
46 palpable tumours 5 – 10 mm in diameter. Micelles of varying antibody densities (0, 5, 10, 15,
47
48 25, 50, 75, and 100%) were diluted in PBS to 2.5 mg mL^{-1} , 100 μL of samples were
49
50 administered I.V. injections *via* the tail vein. To investigate the accumulation of micelles into
51
52 the tumour, mice were sacrificed after 24 and 48 h; PC3-PIP, PC3 tumour and the major organs
53
54
55
56
57
58
59
60

1
2
3 (kidney, liver, spleen, GUT, lung, heart) of all animals were harvested and imaged immediately
4 using IVIS Lumina X5 imaging system (PerkinElmer Inc., Waltham, MA, USA) and analyzed
5 using the Living Image software (PerkinElmer Inc.). The $620_{\text{Ex}}/670_{\text{Em}}$ was used to analyze Cy5
6 fluorescence by micelles. The fluorescence intensities were normalised with respect to the
7 100% antibody-containing micelles, which has been accounted for in Table S1.
8
9

10
11
12
13
14 **Immune cell activation analysis with mice immune cells.** Flow cytometry analysis were
15 carried out according to the protocol by Brown *et al.*⁶¹ Single-cell suspensions from adult
16 spleen or a single lobe of liver were prepared by mechanical dissociation and straining cells
17 through a 70 μm nylon strainer, using a sterile syringe plunger, into tubes containing tonicity-
18 phosphate-buffered saline/2% fetal calf serum (PBS). Single-cell suspensions of spleen or liver
19 containing immune cells of interest were pre-incubated with FVS (live-dead stain, BD
20 Horizon™) for 20 min at room temperature in the dark, followed by blocking with Fc block
21 (1% TruStain fcX™ (anti-mouse CD16/32; BioLegend) in PBS containing 5% rat serum) for
22 10 min to block Fc receptor binding prior to surface staining with antibodies to mouse CD45,
23 F4/80 and CD11b (BioLegend) for 1 h on ice in the dark. Cells were analyzed on a Fortessa
24 X20 flow cytometer (BD Biosciences, Franklin Lakes, NJ) followed by data analysis with
25 FlowJo software (Tree Star, 156 Inc., Ashland, OR). Furthermore, the immune cell analysis of
26 mice blood cells *ex vivo* were also analysed. Micelles with varying antibody densities were
27 added to mice blood samples and the samples were incubated for 1 h at 37 °C. Red blood cells
28 were lysed and cells were phenotyped on ice for 30 min using titrated concentrations of
29 antibodies against CD11b, Ly6G, CD3 and CD19 (BioLegend). Cells were analyzed on a
30 Fortessa X20 flow cytometer (BD Biosciences, Franklin Lakes, NJ) followed by data analysis
31 with FlowJo software (Tree Star, 156 Inc., Ashland, OR).
32
33
34
35
36
37
38
39
40
41
42
43
44
45
46
47
48
49
50
51
52
53
54
55
56
57
58
59
60

1
2
3 **Immune cell activation analysis with Human White Blood Cells.** Fresh blood was collected
4 from a healthy human volunteer (47 year old Female) into sodium heparin vacuettes (Greiner
5 Bio-One) after obtaining informed consent in accordance with the University of Melbourne
6 Human ethics approval 1647326.1 and the Australian National Health and Medical Research
7 Council Statement on Ethical Conduct in Human Research. Micelles with varying antibody
8 densities were added to human blood samples, such that their concentration in blood was 2 μg
9 mL^{-1} , and the samples were incubated for 1 h at 37 °C. Red blood cells were lysed by adding
10 Pharm Lyse buffer (BD) and incubated for 15-30 min in ice and washed twice with PBS (500
11 g, 7 min). Cells were phenotyped on ice for 30 min using titrated concentrations of antibodies
12 against CD66b BV421 (G10F5, BD), CD14 APC-H7 (MΦP9, BD), CD19 BV650 (HIB19,
13 Biolegend), CD3 AF700 (SP34-2, BD), CD56 PE (B159, BD), HLA-DR PerCP-Cy5.5 (G46-
14 6, BD), lineage-1 cocktail FITC (BD). Unbound antibodies were removed by washing and
15 centrifugation (500 g, 7 min) with a cold (4 °C) PBS buffer containing 0.5% w/v BSA and 2
16 mM EDTA. Cells were fixed in 1% w/v formaldehyde in PBS. The samples were directly used
17 for cell association analysis by flow cytometry. The data were processed using FlowJo
18 software.

39 **Statistical analysis**

40 Data for each measurement represent mean \pm standard deviation, n = 3. Statistical analysis was
41 performed using Graphpad Prism 8.1 software. The statistical comparisons were conducted
42 using One-way ANOVA or Two-way ANOVA, followed by the Tukey multicomparison test.
43 P values < 0.05 were considered statistically significant (* = p < 0.05, ** = p < 0.01, *** = p <
44 0.001, **** = p < 0.0001).

56 **ASSOCIATED CONTENT**

Supporting Information

Supporting Information is available free of charge at <http://pubs.acs.org/doi/10.1021/xxxxx>

¹H NMR of polymer precursors, turbidity scans showing LCST behaviour of polymers, SDS-PAGE conjugate analysis, DLS size data of mPEG and scFv, cell association assays for conjugates, DLS size data of conjugates in serum, DLS size, zeta and stability analysis of micelles, competition assay of the micelles, fluorescence images of organs following injection of various constructs, micelle interaction with serum proteins in serum, interaction of micelles with immune cells in mice blood

Financial Interest Statement

The authors declare no competing financial interest.

AUTHOR INFORMATION

Corresponding Author

* E-mail: k.thurecht@uq.edu.au

ORCID

Amal J Sivaram: 0000-0002-6046-3272

Andri Wardiana: 0000-0003-1335-1320

Sheilajen Alcantara

Stefan E. Sonderegger: 0000-0001-9873-0885

Nicholas L. Fletcher: 0000-0002-2993-833X

1
2
3 Zachary H. Houston: 0000-0001-9738-4917
4
5

6 Christopher B. Howard: 0000-0001-9797-8686
7
8

9 Stephen M. Mahler: 0000-0003-2403-1437
10
11

12 Cameron Alexander: 0000-0001-8337-1875
13
14

15 Stephen J. Kent: 0000-0002-8539-4891
16
17

18 Craig A. Bell: 0000-0002-8986-2795
19
20

21 Kristofer J. Thurecht: 0000-0002-4100-3131
22
23

24 **Author Contributions**

25
26
27
28 A.J.S, C.A.B, and K.J.T conceived the project. A.J.S and C.A.B designed the polymer synthesis
29 and characterisations. A.W, C.B.H and S.M.M designed the scFv synthesis. S.A and S.J.K
30 designed the human blood analysis, S.E.S designed the mice immune cell activation analysis.
31
32
33 N.L.F and Z.H.H designed the *in vivo* biodistribution studies. All the authors analysed the data.
34
35
36
37 The manuscript was written through contributions of all authors. All authors have given
38 approval to the final version of the manuscript.
39
40
41

42 **ACKNOWLEDGEMENTS**

43
44
45 The authors acknowledge the facilities, and the scientific and technical assistance of the
46 National Imaging Facility at the Centre for Advanced Imaging, University of Queensland.
47
48 Funding for this research is acknowledged from the National Health and Medical Research
49 Council (APP1099321 and APP1148582 (K.J.T.); APP1054569 (C.A.B.)) and the Australian
50 Research Council (LP150100703 (K.J.T.)). This work was performed in part at the Queensland
51
52
53
54
55
56
57
58
59
60 node of the Australian National Fabrication Facility (ANFF), a company established under the

1
2
3 National Collaborative Research Infrastructure Strategy to provide nano- and microfabrication
4 facilities for Australia's researchers. This research was conducted and funded by the ARC
5
6 Centre of Excellence in Convergent Bio-Nano Science and Technology (CE140100036) and
7
8 in part by the ARC Training Centre for Innovation in Biomedical Imaging Technologies
9
10 (IC170100035).
11
12
13

14 15 REFERENCES

- 16
17
18 1. Shi, J.; Kantoff, P. W.; Wooster, R.; Farokhzad, O. C., Cancer Nanomedicine: Progress,
19 Challenges and Opportunities. *Nat. Rev. Cancer* **2017**, *17*, 20-37.
20
21
- 22
23 2. Wicki, A.; Witzigmann, D.; Balasubramanian, V.; Huwyler, J., Nanomedicine in
24 Cancer Therapy: Challenges, Opportunities, and Clinical Applications. *J. Controlled Release*
25 **2015**, *200*, 138-157.
26
27
- 28
29 3. Muthu, M. S.; Leong, D. T.; Mei, L.; Feng, S.-S., Nanotheranostics - Application and
30 Further Development of Nanomedicine Strategies for Advanced Theranostics. *Theranostics*
31 **2014**, *4*, 660-677.
32
33
- 34
35 4. Wilhelm, S.; Tavares, A. J.; Dai, Q.; Ohta, S.; Audet, J.; Dvorak, H. F.; Chan, W. C.,
36 Analysis of Nanoparticle Delivery to Tumours. *Nat. Rev. Mater.* **2016**, *1*, 16014.
37
38
- 39
40 5. Fang, J.; Nakamura, H.; Maeda, H., The EPR Effect: Unique Features of Tumor Blood
41 Vessels for Drug Delivery, Factors Involved, and Limitations and Augmentation of the Effect.
42 *Adv. Drug Delivery Rev.* **2011**, *63*, 136-151.
43
44
- 45
46 6. Bjornmalm, M.; Thurecht, K. J.; Michael, M.; Scott, A. M.; Caruso, F., Bridging Bio-
47 Nano Science and Cancer Nanomedicine. *ACS Nano* **2017**, *11*, 9594-9613.
48
49
- 50
51 7. Yoo, J.-W.; Chambers, E.; Mitragotri, S., Factors That Control the Circulation Time of
52 Nanoparticles in Blood: Challenges, Solutions and Future Prospects. *Curr. Pharm. Des.* **2010**,
53 *16*, 2298-2307.
54
55
56
57
58
59
60

- 1
2
3 8. Zhang, S.; Li, J.; Lykotrafitis, G.; Bao, G.; Suresh, S., Size-Dependent Endocytosis of
4 Nanoparticles. *Adv. Mater.* **2009**, *21*, 419-424.
5
6
- 7
8 9. Cui, J.; Ju, Y.; Houston, Z. H.; Glass, J. J.; Fletcher, N. L.; Alcantara, S.; Dai, Q.;
9
10 Howard, C. B.; Mahler, S. M.; Wheatley, A. K.; De Rose, R.; Brannon, P. T.; Paterson, B. M.;
11
12 Donnelly, P. S.; Thurecht, K. J.; Caruso, F.; Kent, S. J., Modulating Targeting of Poly(Ethylene
13
14 Glycol) Particles to Tumor Cells Using Bispecific Antibodies. *Adv. Healthcare Mater.* **2019**,
15
16 8, 1801607.
17
- 18
19 10. Alkilany, A. M.; Zhu, L.; Weller, H.; Mews, A.; Parak, W. J.; Barz, M.; Feliu, N.,
20
21 Ligand Density on Nanoparticles: A Parameter with Critical Impact on Nanomedicine. *Adv.*
22
23 *Drug Delivery Rev.* **2019**, *143*, 22-36.
24
- 25
26 11. Pelaz, B.; del Pino, P.; Maffre, P.; Hartmann, R.; Gallego, M.; Rivera-Fernandez, S.;
27
28 de la Fuente, J. M.; Nienhaus, G. U.; Parak, W. J., Surface Functionalization of Nanoparticles
29
30 with Polyethylene Glycol: Effects on Protein Adsorption and Cellular Uptake. *ACS Nano* **2015**,
31
32 9, 6996-7008.
33
- 34
35 12. Moody, P. R.; Sayers, E. J.; Magnusson, J. P.; Alexander, C.; Borri, P.; Watson, P.;
36
37 Jones, A. T., Receptor Crosslinking: A General Method to Trigger Internalization and
38
39 Lysosomal Targeting of Therapeutic Receptor: Ligand Complexes. *Mol. Ther.* **2015**, *23*, 1888-
40
41 1898.
42
- 43
44 13. Colombo, M.; Fiandra, L.; Alessio, G.; Mazzucchelli, S.; Nebuloni, M.; De Palma, C.;
45
46 Kantner, K.; Pelaz, B.; Rotem, R.; Corsi, F.; Parak, W. J.; Prospero, D., Tumour Homing and
47
48 Therapeutic Effect of Colloidal Nanoparticles Depend on the Number of Attached Antibodies.
49
50 *Nat. Commun.* **2016**, *7*, 13818.
51
- 52
53 14. Sayers, E. J.; Magnusson, J. P.; Moody, P. R.; Mastrotto, F.; Conte, C.; Brazzale, C.;
54
55 Borri, P.; Caliceti, P.; Watson, P.; Mantovani, G.; Aylott, J.; Salmaso, S.; Jones, A. T.;
56
57
58
59
60

- Alexander, C., Switching of Macromolecular Ligand Display by Thermoresponsive Polymers Mediates Endocytosis of Multiconjugate Nanoparticles. *Bioconjugate Chem.* **2018**, *29*, 1030-1046.
15. Makwana, H.; Mastrotto, F.; Magnusson, J. P.; Sleep, D.; Hay, J.; Nicholls, K. J.; Allen, S.; Alexander, C., Engineered Polymer-Transferrin Conjugates as Self-Assembling Targeted Drug Delivery Systems. *Biomacromolecules* **2017**, *18*, 1532-1543.
16. Poon, Z.; Chen, S.; Engler, A. C.; Lee, H. i.; Atas, E.; von Maltzahn, G.; Bhatia, S. N.; Hammond, P. T., Ligand-Clustered "Patchy" Nanoparticles for Modulated Cellular Uptake and *In Vivo* Tumor Targeting. *Angew. Chem.* **2010**, *49*, 7266-7270.
17. Griebenow, K.; Klibanov, A. M., On Protein Denaturation in Aqueous-Organic Mixtures But Not in Pure Organic Solvents. *J. Am. Chem. Soc.* **1996**, *118*, 11695-11700.
18. Koo, H.; Lee, S.; Na, J. H.; Kim, S. H.; Hahn, S. K.; Choi, K.; Kwon, I. C.; Jeong, S. Y.; Kim, K., Bioorthogonal Copper-Free Click Chemistry *In Vivo* for Tumor-Targeted Delivery of Nanoparticles. *Angew. Chem.* **2012**, *51*, 11836-11840.
19. Gibson, M. I.; Fröhlich, E.; Klok, H. A., Postpolymerization Modification of Poly(Pentafluorophenyl Methacrylate): Synthesis of a Diverse Water-Soluble Polymer Library. *J. Polym. Sci., Part A: Polym. Chem.* **2009**, *47*, 4332-4345.
20. Kim, D. W.; Ahn, D.-S.; Oh, Y.-H.; Lee, S.; Kil, H. S.; Oh, S. J.; Lee, S. J.; Kim, J. S.; Ryu, J. S.; Moon, D. H.; Chi, D. Y., A New Class of SN2 Reactions Catalyzed by Protic Solvents: Facile Fluorination for Isotopic Labeling of Diagnostic Molecules. *J. Am. Chem. Soc.* **2006**, *128*, 16394-16397.
21. Gyarmati, B.; Némethy, Á.; Szilágyi, A., Reversible Disulphide Formation in Polymer Networks: A Versatile Functional Group From Synthesis to Applications. *Eur. Polym. J.* **2013**, *49*, 1268-1286.

- 1
2
3 22. Wang, C.; Yan, Q.; Liu, H.-B.; Zhou, X.-H.; Xiao, S.-J., Different EDC/NHS
4 Activation Mechanisms between PAA and PMAA Brushes and the Following Amidation
5 Reactions. *Langmuir* **2011**, *27*, 12058-12068.
6
7
8
9
10 23. Smith-Jones, P. M.; Vallabhajosula, S.; Navarro, V.; Bastidas, D.; Goldsmith, S. J.;
11 Bander, N. H., Radiolabeled Monoclonal Antibodies Specific to the Extracellular Domain of
12 Prostate-Specific Membrane Antigen: Preclinical Studies in Nude Mice Bearing LNCaP
13 Human Prostate Tumor. *J. Nucl. Med.* **2003**, *44*, 610-617.
14
15
16
17
18
19 24. Lang, K.; Chin, J. W., Cellular Incorporation of Unnatural Amino Acids and
20 Bioorthogonal Labeling of Proteins. *Chem. Rev.* **2014**, *114*, 4764-4806.
21
22
23
24 25. Sayers, C. T.; Mantovani, G.; Ryan, S. M.; Randev, R. K.; Keiper, O.; Leszczyszyn, O.
25 I.; Blindauer, C.; Brayden, D. J.; Haddleton, D. M., Site-Specific N-Terminus Conjugation of
26 Poly(mPEG 1100) Methacrylates to Salmon Calcitonin: Synthesis and Preliminary Biological
27 Evaluation. *Soft Matter* **2009**, *5*, 3038-3046.
28
29
30
31
32
33 26. Decker, C. G.; Maynard, H. D., Degradable PEGylated Protein Conjugates Utilizing
34 RAFT Polymerization. *Eur. Polym. J.* **2015**, *65*, 305-312.
35
36
37
38 27. Samanta, D.; McRae, S.; Cooper, B.; Hu, Y.; Emrick, T.; Pratt, J.; Charles, S. A., End-
39 Functionalized Phosphorylcholine Methacrylates and Their Use in Protein Conjugation.
40 *Biomacromolecules* **2008**, *9*, 2891-2897.
41
42
43
44 28. Caster, J. M.; Patel, A. N.; Zhang, T.; Wang, A., Investigational Nanomedicines in
45 2016: A Review of Nanotherapeutics Currently Undergoing Clinical Trials. *Wiley Interdiscip.*
46 *Rev.: Nanomed. Nanobiotechnol.* **2017**, *9*, e1416.
47
48
49
50
51 29. Chuang, K.-H.; Kao, C.-H.; Roffler, S. R.; Lu, S.-J.; Cheng, T.-C.; Wang, Y.-M.;
52 Chuang, C.-H.; Hsieh, Y.-C.; Wang, Y.-T.; Wang, J.-Y.; Weng, K.-Y.; Cheng, T.-L.,
53
54
55
56
57
58
59
60

1
2
3 Development of an Anti-Methoxy Poly(Ethylene Glycol)(α -mPEG) Cell-Based Capture
4 System to Measure mPEG and mPEGylated Molecules. *Macromolecules* **2014**, *47*, 6880-6888.

5
6
7
8 30. Ghosh, A.; Heston, W. D., Tumor Target Prostate Specific Membrane Antigen (PSMA)
9 and Its Regulation in Prostate Cancer. *J. Cell. Biochem.* **2004**, *91*, 528-539.

10
11
12 31. Rapoport, N., Physical Stimuli-Responsive Polymeric Micelles for Anti-Cancer Drug
13 Delivery. *Prog. Polym. Sci.* **2007**, *32*, 962-990.

14
15
16 32. van Nostrum, C. F., Covalently Cross-Linked Amphiphilic Block Copolymer Micelles.
17 *Soft Matter* **2011**, *7*, 3246-3259.

18
19
20
21 33. Eliezar, J.; Scarano, W.; Boase, N. R.; Thurecht, K. J.; Stenzel, M. H., *In Vivo*
22 Evaluation of Folate Decorated Cross-Linked Micelles for the Delivery of Platinum Anticancer
23 Drugs. *Biomacromolecules* **2015**, *16*, 515-523.

24
25
26 34. Hu, Z.; Cai, T.; Chi, C., Thermoresponsive Oligo(Ethylene Glycol)-Methacrylate-
27 Based Polymers and Microgels. *Soft Matter* **2010**, *6*, 2115-2123.

28
29
30
31 35. Chanakira, A.; Chikwana, E.; Peyton, D. H.; Simoyi, R. H., Oxyhalogen-Sulfur
32 Chemistry - Kinetics and Mechanism of the Oxidation of Cysteamine by Acidic Iodate and
33 Iodine. *Can. J. Chem.* **2006**, *84*, 49-57.

34
35
36
37 36. Steinhauer, W.; Keul, H.; Möller, M., Synthesis of Reversible and Irreversible Cross-
38 Linked (M)PEG-(meth)acrylate Based Functional Copolymers. *Polym. Chem.* **2011**, *2*, 1803-
39 1814.

40
41
42
43 37. Elias, D. R.; Poloukhine, A.; Popik, V.; Tsourkas, A., Effect of Ligand Density,
44 Receptor Density, and Nanoparticle Size on Cell Targeting. *Nanomedicine (N. Y., NY, U. S.)*
45 **2013**, *9*, 194-201.

46
47
48
49 38. Yuan, H.; Li, J.; Bao, G.; Zhang, S., Variable Nanoparticle-Cell Adhesion Strength
50 Regulates Cellular Uptake. *Phys. Rev. Lett.* **2010**, *105*, 138101.

- 1
2
3 39. Thurber, G. M.; Weissleder, R., Quantitating Antibody Uptake *In Vivo*: Conditional
4 Dependence on Antigen Expression Levels. *Mol. Imaging Biol.* **2011**, *13*, 623-632.
5
6
7
8 40. Such, G. K.; Johnston, A. P., Understanding Cell Interactions Using Modular
9 Nanoparticle Libraries. *Aust. J. Chem.* **2019**, *72*, 595-599.
10
11
12 41. Zern, B. J.; Chacko, A.-M.; Liu, J.; Greineder, C. F.; Blankemeyer, E. R.;
13 Radhakrishnan, R.; Muzykantov, V., Reduction of Nanoparticle Avidity Enhances the
14 Selectivity of Vascular Targeting and PET Detection of Pulmonary Inflammation. *ACS Nano*
15 **2013**, *7*, 2461-2469.
16
17
18
19
20
21 42. Caré, B. R.; Soula, H. A., Impact of Receptor Clustering on Ligand Binding. *BMC Syst.*
22 *Biol.* **2011**, *5*, 1-13.
23
24
25
26 43. Schmidt, D.; Bihl, T.; Fenz, S.; Merkel, R.; Seifert, U.; Sengupta, K.; Smith, A.-S.,
27 Crowding of Receptors Induces Ring-Like Adhesions in Model Membranes. *Biochim. Biophys.*
28 *Acta, Mol. Cell Res.* **2015**, *1853*, 2984-2991.
29
30
31
32
33 44. Yong, K. W.; Yuen, D.; Chen, M. Z.; Johnston, A. P., Engineering the Orientation,
34 Density, and Flexibility of Single-Domain Antibodies on Nanoparticles to Improve Cell
35 Targeting. *ACS Appl. Mater. Interfaces* **2020**, *12*, 5593-5600.
36
37
38
39
40 45. Xu, S.; Olenyuk, B. Z.; Okamoto, C. T.; Hamm-Alvarez, S. F., Targeting Receptor-
41 Mediated Endocytotic Pathways with Nanoparticles: Rationale and Advances. *Adv. Drug*
42 *Delivery Rev.* **2013**, *65*, 121-138.
43
44
45
46 46. Liu, A. P.; Aguet, F.; Danuser, G.; Schmid, S. L., Local Clustering of Transferrin
47 Receptors Promotes Clathrin-Coated Pit Initiation. *J. Cell Biol.* **2010**, *191*, 1381-1393.
48
49
50
51 47. Rosenblum, D.; Joshi, N.; Tao, W.; Karp, J. M.; Peer, D., Progress and Challenges
52 towards Targeted Delivery of Cancer Therapeutics. *Nat. Commun.* **2018**, *9*, 1410.
53
54
55
56
57
58
59
60

- 1
2
3 48. Shi, C.; Pamer, E. G., Monocyte Recruitment During Infection and Inflammation. *Nat.*
4
5 *Rev. Immunol.* **2011**, *11*, 762-774.
6
7
8 49. Schaller, E.; Macfarlane, A. J.; Rupec, R. A.; Gordon, S.; McKnight, A. J.; Pfeffer, K.,
9
10 Inactivation of the F4/80 Glycoprotein in the Mouse Germ Line. *Mol. Cell. Biol.* **2002**, *22*,
11
12 8035-8043.
13
14
15 50. Poon, W.; Zhang, Y.-N.; Ouyang, B.; Kingston, B. R.; Wu, J. L.; Wilhelm, S.; Chan,
16
17 W. C., Elimination Pathways of Nanoparticles. *ACS Nano* **2019**, *13*, 5785–5798.
18
19
20 51. Walkey, C. D.; Chan, W. C., Understanding and Controlling the Interaction of
21
22 Nanomaterials with Proteins in a Physiological Environment. *Chem. Soc. Rev.* **2012**, *41*, 2780-
23
24 2799.
25
26
27 52. Weiss, A. C.; Kelly, H. G.; Faria, M.; Besford, Q. A.; Wheatley, A. K.; Ang, C.-S.;
28
29 Crampin, E. J.; Caruso, F.; Kent, S. J., Link between Low-Fouling and Stealth: A Whole Blood
30
31 Biomolecular Corona and Cellular Association Analysis on Nanoengineered Particles. *ACS*
32
33 *Nano* **2019**, *13*, 4980-4991.
34
35
36 53. Tenzer, S.; Docter, D.; Kuharev, J.; Musyanovych, A.; Fetz, V.; Hecht, R.; Schlenk, F.;
37
38 Fischer, D.; Kiouptsi, K.; Reinhardt, C.; Landfester, K.; Schild, H.; Maskos, M.; Knauer, S.
39
40 K.; Stauber, R. H., Rapid Formation of Plasma Protein Corona Critically Affects Nanoparticle
41
42 Pathophysiology. *Nat. Nanotechnol.* **2013**, *8*, 772-781.
43
44
45 54. Walkey, C. D.; Olsen, J. B.; Song, F.; Liu, R.; Guo, H.; Olsen, D. W. H.; Cohen, Y.;
46
47 Emili, A.; Chan, W. C., Protein Corona Fingerprinting Predicts the Cellular Interaction of Gold
48
49 and Silver Nanoparticles. *ACS Nano* **2014**, *8*, 2439-2455.
50
51
52 55. Boraschi, D.; Italiani, P.; Palomba, R.; Decuzzi, P.; Duschl, A.; Fadeel, B.; Moghimi,
53
54 S. M., Nanoparticles and Innate Immunity: New Perspectives on Host Defence. *Semin.*
55
56 *Immunol.* **2017**, *34*, 33-51.
57
58
59
60

- 1
2
3 56. Glass, J. J.; Chen, L.; Alcantara, S.; Crampin, E. J.; Thurecht, K. J.; De Rose, R.; Kent,
4 S. J., Charge Has a Marked Influence on Hyperbranched Polymer Nanoparticle Association in
5 Whole Human Blood. *ACS Macro Lett.* **2017**, *6*, 586-592.
6
7
8
9
10 57. Fuchs, A. V.; Tse, B. W.; Pearce, A. K.; Yeh, M. C.; Fletcher, N. L.; Huang, S. S.;
11 Heston, W. D.; Whittaker, A. K.; Russell, P. J.; Thurecht, K. J., Evaluation of Polymeric
12 Nanomedicines Targeted to PSMA: Effect of Ligand on Targeting Efficiency.
13 *Biomacromolecules* **2015**, *16*, 3235-47.
14
15
16
17
18 58. Convertine, A. J.; Benoit, D. S.; Duvall, C. L.; Hoffman, A. S.; Stayton, P. S.,
19 Development of a Novel Endosomolytic Diblock Copolymer for siRNA Delivery. *J.*
20 *Controlled Release* **2009**, *133*, 221-229.
21
22
23
24
25
26 59. Nakajima, T.; Mitsunaga, M.; Bander, N. H.; Heston, W. D.; Choyke, P. L.; Kobayashi,
27 H., Targeted, Activatable, *In Vivo* Fluorescence Imaging of Prostate-Specific Membrane
28 Antigen (PSMA) Positive Tumors Using the Quenched Humanized J591 Antibody–
29 Indocyanine Green (ICG) Conjugate. *Bioconjugate Chem.* **2011**, *22*, 1700-1705.
30
31
32
33
34
35 60. Faria, M.; Björnmalm, M.; Thurecht, K. J.; Kent, S. J.; Parton, R. G.; Kavallaris, M.;
36 Johnston, A. P.; Gooding, J. J.; Corrie, S. R.; Boyd, B. J.; Thordarson, P.; Whittaker, A. K.;
37 Stevens, M. M.; Prestidge, C. A.; Porter, C. J. H.; Parak, W. J.; Davis, T. P.; Crampin, E. J.;
38 Caruso, F., Minimum Information Reporting in Bio–Nano Experimental Literature. *Nat.*
39 *Nanotechnol.* **2018**, *13*, 777-785.
40
41
42
43
44
45 61. Brown, F. C.; Scott, N.; Rank, G.; Collinge, J. E.; Vadolas, J.; Vickaryous, N.;
46 Whitelaw, N.; Whitelaw, E.; Kile, B. T.; Jane, S. M.; Curtis, D. J., ENU Mutagenesis Identifies
47 the First Mouse Mutants Reproducing Human β -Thalassemia at the Genomic Level. *Blood*
48 *Cells, Mol., Dis.* **2013**, *50*, 86-92.
49
50
51
52
53
54
55
56
57
58
59
60

TOC Graphic

